frontiers | Frontiers in Marine Science

TYPE Original Research
PUBLISHED 20 December 2024
DOI 10.3389/fmars.2024.1473237

OPEN ACCESS

EDITED BY
Juan Jose Munoz-Perez,
University of Cádiz, Spain

REVIEWED BY
Francisco Contreras de Villar,
University of Cádiz, Spain
Jose Maria Del Campo,
Polytechnic University of Madrid, Spain

*CORRESPONDENCE
Jan Tiede
tiede@lufi.uni-hannover.de

RECEIVED 30 July 2024
ACCEPTED 18 November 2024
PUBLISHED 20 December 2024

CITATION
Tiede J, Jordan C, Siewert M, Sommermeier K and Schlurmann T (2024) Evolution of beach profiles at the German Baltic Sea during and after large-scale beach nourishment: bar formation and sand redistribution.
Front. Mar. Sci. 11:1473237.
doi: 10.3389/fmars.2024.1473237

Evolution of beach profiles at the German Baltic Sea during and after large-scale beach nourishment: bar formation and sand redistribution

Jan Tiede[1*], Christian Jordan[1], Marcus Siewert[2], Knut Sommermeier[2] and Torsten Schlurmann[1]

[1]Ludwig-Franzius-Institute, Leibniz University Hanover, Hanover, Germany, [2]Mecklenburg-Vorpommern State Agency of Agriculture and Environment, Department Coast, Rostock, Germany

Coastal zones, critical for their ecological and economic significance, are increasingly vulnerable to storm surges, sea-level rise, and land subsidence. Traditional defense mechanisms, such as dikes and seawalls, are often costly and environmentally taxing. This research highlights how beach and dune systems, key components of coastal protection in the Baltic Sea region, evolve following sand nourishment. Dunes, sustained by periodic sand replenishments, play a critical role in shielding the coast from storm surges, high water levels, and erosion. High-resolution data from Unmanned Aerial Vehicle surveys, alongside terrestrial field observations, provide insights into the morphological changes post-nourishment, including the formation and dynamics of sandbars. Additionally, we demonstrate how UAV photogrammetry can achieve significantly improved change detection through advanced co-alignment techniques, resulting in enhanced precision and reliability of the data. The study underscores the importance of dunes and sandbars in mitigating erosion and advocates for their continued inclusion in coastal protection strategies. The results emphasize the need for long-term monitoring and adaptive management to optimize nourishment effectiveness, supporting sustainable coastal development and resilience against future challenges.

KEYWORDS

photogrammetry, RTK UAV, sand nourishment, co-alignment, coastal dynamics, bathymetry, bar morphodynamics

Introduction

Being at the interface between water and land, coastal zones host marine resources, infrastructure, and potential for tourism while also providing ecosystem services (European Commission, 2022). However, these areas are increasingly threatened by storm surges, sea-level rise (SLR), and land subsidence, which can lead to erosion and flooding (Oppenheimer et al., 2019). Traditional coastal defenses, such as dikes, seawalls, and embankments, are commonly used but come with high costs and environmental drawbacks (Schoonees et al., 2019). As sea levels rise, these methods require continuous re-enforcing, becoming unsustainable over time. In contrast, dunes offer a more adaptive solution, providing critical ecosystem services (Everard et al., 2010) and the ability to adjust naturally in response to changing conditions (Barbier et al., 2011). However, dunes require regular replenishment to counteract sand loss caused by metocean forces, a necessity that is particularly pronounced in highly erosive regions. In this context, sand nourishments stand out as a central element of a sustainable and flexible coastal protection strategy. This approach focuses on replenishing coastal zones experiencing erosion with nourishments, while also installing additional structures to stabilize the sand. As Staudt et al. (2021) pointed out, beach nourishments are a widely used method to mitigate erosion along sandy shorelines and are considered soft engineering. The adaptability of nourished beach-dune systems to the varying scenarios of SLR, as outlined by Oppenheimer et al. (2019), reinforces their reputation as flexible, beneficial to ecosystems, and reliable.

Since the cumulative, long-term environmental impacts of marine sediment extraction and nourishment activities are not yet fully understood, efforts have been made to understand the drivers behind the long-term and large-scale behavior of coasts (Mentaschi et al., 2018). It is hypothesized that so called large-scale coastal behavior regions (LSCB-regions) exist, which are controlled by the same drivers (e.g. hydrodynamic or morphological). For example, such LSCB-regions were successfully identified along the Dutch coast, though clear signals in the long-term development of sub-aqueous profiles could not be observed (Wijnberg and Terwindt, 1995). However, it was shown that (sub)decadal shoreline fluctuations may be connected to the large-scale dynamics of multiple bar systems. It is also commonly inferred that SLR and altered wave action due to climate change contribute to long-term coastal erosion and development. However, establishing a clear link between these phenomena and field or hindcast data has proven challenging. Ghanavati et al. (2023), for example, attempted to address this issue but did not achieve conclusive results.

SLR will also lead to a future increase in sand volumes needed for beach nourishments. In line with this, previous studies have estimated the future sand volumes required for beach nourishment to mitigate the effects of SLR. In line with this, Aguilera-Vidal et al. (2022) used the Bruun Rule to estimate shoreline retreat due to SLR and subsequently calculated the sand volume necessary to renourish the beach and counteract this retreat. Their findings indicate that, under the most pessimistic SLR projections, the annual sand volume needed for nourishment at Victoria Beach in the Gulf of Cadiz could double, underscoring the substantial challenges that future SLR could impose on coastal management strategies.

In general, the evolution of a nourishment is intricately tied to a multitude of factors. Primarily, the incoming wave energy forces a nourishment to transition towards a more natural state i.e. the so-called equilibrium beach profile (Bruun, 1954; Dean, 1977). The transition is forced by longshore and cross-shore redistribution of the sediment, both of which are predominantly dependent on the dynamics of incoming wave energy. For a more detailed assessment of the intricate changes, the angle of wave attack, coastal topography, sediment composition, profile specifications, and engineered structures must be included (Leach et al., 2023). The singular most prominent feature of the nearshore morphology is sandbars; their interaction with the subaerial beach takes place by several mechanisms and on a multitude of time scales. Several researchers have studied the different mechanisms by which the development of the sand bars and of the subaerial beach and foredune are linked to each other. They investigated the correlation between short-term and mid-term variations in shoreline and sediment volume on subaerial beaches and the cyclic fluctuations in sandbar systems during net offshore migration (Shand, 2003; Yuhi and Umeda, 2018; Melito et al., 2018). They also observed the supply of beach sediment from sandbar welding (Aagaard et al., 2006; Cohn et al., 2015) and the interplay between shoreline and sandbar behavior (Gijsman et al., 2021). Despite significant research efforts in this area, our understanding of the connections between subaerial beaches and subaqueous sandbars continues to evolve.

Recent studies on the development of freshly nourished beaches and dunes under wave impact have shed light on the planform and cross-shore adaption of the beach profile (Dean, 2002). The planform adaption results in sediment accumulation in the beaches adjacent to the nourishment. Though this process is largely symmetrical, Ludka et al. (2023) showed that it can also be an asymmetrical process with the wave direction being the controlling factor. The other redistribution process happens in the cross-shore profile. Elko and Wang (2007) identified the initial occurrence of cross-shore redistribution to be primarily governed by high-energy wave activity. The consensus is that the redistribution happens largely in the first months or year after the completion of the nourishment (Browder and Dean, 2000). Initially, the redistribution will be seawards, with sediment from the subaerial beach moving downslope. In the past, researchers have employed a combination of field measurements (McGill et al., 2022), remote sensing techniques (Vos et al., 2019), and numerical modeling (Luijendijk et al., 2017) to analyze the behavior of these nourishments over time, observing the evolution of coastal profiles, sediment transport, and erosion patterns.

A significant area of research about beach nourishments has focused on the application of Empirical Orthogonal Function (EOF) analysis to understand beach dynamics. Larson et al. (1999) utilized EOF analysis to study the short- and long-term responses of beach fills, finding that the time required for a beach to stabilize after nourishment is heavily influenced by the placement of the fill material within the active profile, with faster stabilization

occurring when the material is placed within this zone. Muñoz-Pérez et al. (2001) also applied the EOF method to analyze longshore variations in sediment transport and shoreline changes. Their research demonstrated the method's effectiveness in capturing key patterns of variability along coastlines, contributing to more informed and precise beach nourishment designs by better understanding the underlying coastal processes.

In addition to analytical techniques like EOF, advancements in monitoring techniques have significantly improved the assessment of beach nourishment projects. Ojeda and Guillén (2006) employed video monitoring to track the evolution of nourished beaches, providing continuous, detailed observations of shoreline changes. This method offered a dynamic understanding of sediment movement and beach morphology, particularly valuable in capturing rapid changes that traditional survey methods might miss. Gares et al. (2006) further advanced monitoring efforts by using LIDAR technology in a beach nourishment project. The high-resolution data from LIDAR provided precise measurements of beach topography before and after nourishment, showcasing the advantages of such technology for large-scale, repeatable coastal monitoring.

While these technological advancements have enhanced the monitoring and analysis of beach nourishment projects, understanding the environmental impacts of these interventions remains crucial. Peterson and Bishop (2005) assessed the ecological effects of beach nourishments, noting that while they can effectively combat erosion and protect coastal infrastructure, they may also disrupt local ecosystems. Changes in sediment composition and habitat conditions can have significant consequences for local flora and fauna (Saengsupavanich et al., 2023), underscoring the need to carefully consider ecological impacts during the planning and execution of nourishment projects. In estuarine environments, where natural processes and ecosystems are particularly sensitive, Jackson et al. (2010) also found that nourishment projects can significantly alter beach profiles and sediment characteristics, affecting habitat suitability and natural processes like aeolian transport. This research highlights the complex trade-offs involved in using nourishment as a shore protection strategy in sensitive environments.

China's experience with beach nourishment provides valuable insights into the large-scale implementation of these projects. Cai et al. (2011) offered a comprehensive review of the history and current status of beach nourishment in China, categorizing the development of these projects into three stages. Their study illustrates how China has progressively adopted and adapted international best practices to suit its unique coastal conditions. The authors emphasized the need for a national strategy to ensure the long-term sustainability of beach nourishment efforts in China, suggesting that future projects will need to be larger and more systematically planned.

In this study, we focus on a section of the German Baltic Sea coast and the evolution of local beach profiles after a large-scale beach nourishment (Figure 1). Due to the reliance on dunes, sand nourishments are a vital part of the coastal protection strategy of the state of Mecklenburg-Western-Pomerania (MWP) including the study area. In the past, the combination of natural coastal development, coastal infrastructure, and protection measures has complicated the assessment of the effect of these nourishments. The current strategy is to react to the changes seen on the beach and replace the sand that was washed away by the usual sea state and storm impacts. To improve these practices, a deeper understanding of the shoreline dynamics is fundamental for planning the commitment of sand supplies along the coast, especially considering the challenges in the form of SLR lying ahead.

This paper presents a high-resolution analysis of the transient evolution of subaqueous and subaerial beach profiles following a beach and dune nourishment event, focusing on how the nourishment enhances the dune's ability to protect the hinterland. The study explores the generation and influence of sandbars, which induce wave-breaking and potentially mitigate storm-related erosion. To thoroughly assess the effectiveness of the nourishment, a multi-faceted data collection approach was employed, examining both short-term changes during the nourishment and mid-term developments of the beach and dune over the following 25 months. During the nourishment process, detailed measurements of both subaqueous and subaerial beach profiles, as well as the dune, were conducted using a combination of GPS and echo sounder systems. These instruments allowed for accurate assessment of the immediate morphological changes, capturing the role of sandbars in sediment redistribution and the overall impact of the nourishment on the coastal system.

Following the completion of the nourishment, Unmanned Aerial Vehicle (UAV) surveys were conducted over 25 months to monitor the mid-term evolution of the nourished area. The UAV data provided high-resolution insights into how the dune evolved, allowing for an assessment of both its short-term reshaping and mid-term stability, as well as its effectiveness in serving as a barrier against coastal threats. By integrating data from both the nourishment phase and the post-nourishment monitoring, this study offers a comprehensive understanding of how the nourishment enhanced the dune's protective capacity, its effectiveness in mitigating coastal erosion, and its role in safeguarding the hinterland.

Materials and Methods

Study site

The study site lies at the southwestern Baltic Sea, where the predominant coastal protection measure are nourishments. The southwestern Baltic Sea's outer coastline of the federal state of MWP extends over 377 km, with a composition of 237 km of flat coast and 140 km of cliffs. Historical cartographic analyses by governmental bodies reveal that 65% of the coastline is undergoing erosion, 13% is expanding seaward, and 22% remains stable (StALU, 2021). Over a century, the rate of coastal erosion averages 0.35 m per year, though, in certain areas, this rate escalates to as much as 2.1 m annually. Conversely, some regions exhibit accretion rates reaching 4.0 m per year. Cliffs, constituting about one-third of the coastal length, serve as significant sediment sources, enhancing deposition in adjacent zones. For example, the

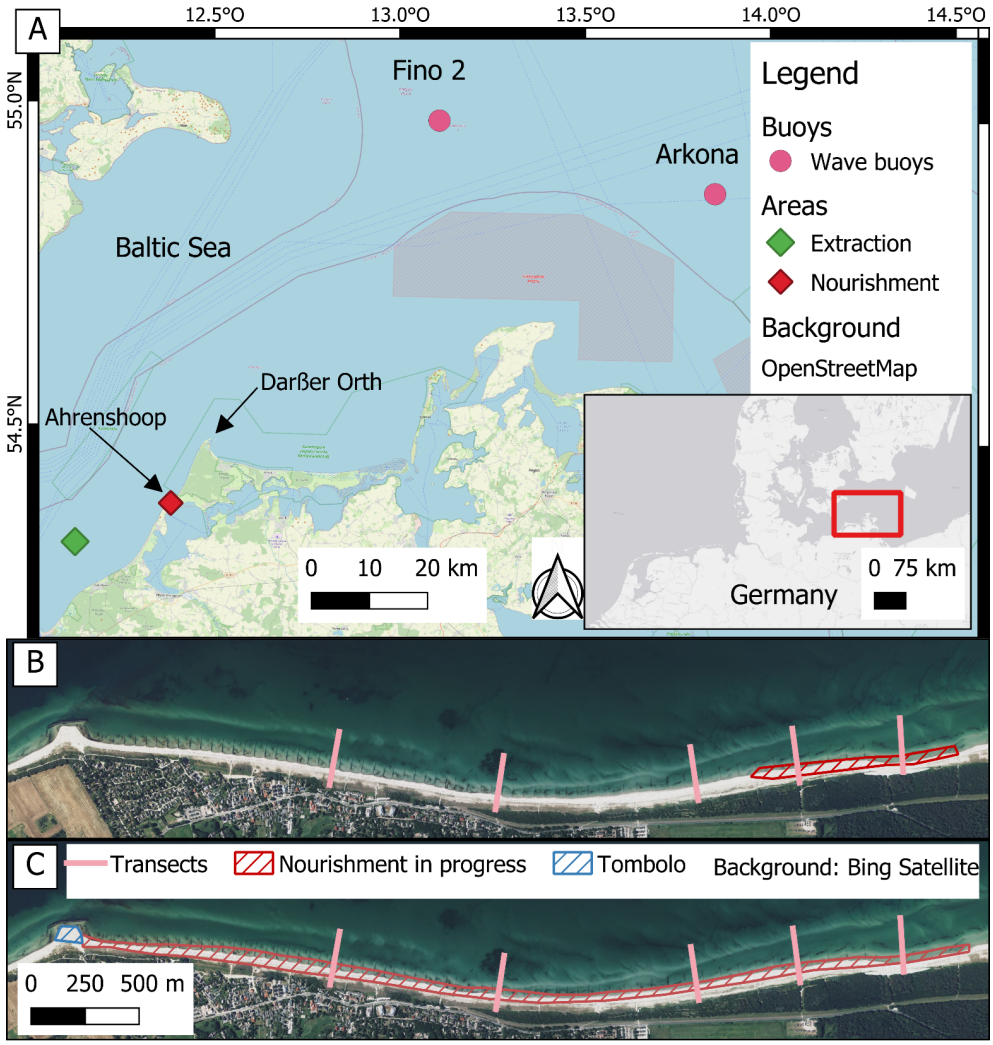

FIGURE 1
(A) Overview of the study area, red rectangle marks the zoomed-in map. **(B)** Aerial view of the nourishment site in Ahrenshoop during the process of nourishing sand to the study area on the 13th of February 2021. **(C)** Aerial view of the completed nourishment on the 1st of March 2021. A small amount of the nourished sand was taken from the tombolo behind the breakwater adjacent to the nourishment, while the bulk marine aggregate was sourced from the extraction site at Graal-Mueritz [see green polygon in **(A)**]. The graphically indicated red areas in **(B, C)** mark the nourished foreshore and beaches. Background map source for panel **(A)**: Map data © OpenStreetMap contributors. For **(B, C)**: Esri, DigitalGlobe, GeoEye, i-cubed, USDA FSA, USGS, AEX, Getmapping, 471 Aerogrid, IGN, IGP, swisstopo, and the GIS User Community.

cliff at Ahrenshoop, known as "Hohes Ufer", is experiencing erosion at a rate of approximately 0.55 m per year. Efforts to conserve these cliffs for tourism and agricultural purposes have inadvertently impacted the adjacent flat coastlines negatively. As a result, most cliffs are left without protection, facilitating their role in sediment provision (StALU, 2021). As of today, the coast of the Baltic Sea is known to demonstrate a natural equilibrium, with erosion predominating in exposed locales and sediment accumulation in protected ones. Behind the primary coastline lie extensive bays, which are only partly open to the sea, where coastal defense measures are reduced in scale due to lower wave height, emphasizing the importance of safeguarding the outer coast against breaches and inundations. Nonetheless, the impact of seasonal variations on this equilibrium and the future sustainability of these erosion and accretion dynamics remain largely unexplored.

The challenges associated with coastal defense efforts due to erosion are strongly believed to be exacerbated by the impacts of climate change and sea level rise (SLR) (Leatherman et al., 2000; Monioudi et al., 2017). Kelln et al. (2022) reported that the sea level in the southwestern Baltic Sea has increased by 1.23 ± 0.11 mm/year from 1900 to 2015, as indicated by tide gauge records. Moreover, recent research indicates a significant acceleration in the rate of SLR. For instance, Madsen et al. (2019) observed an increase in the absolute sea level for the Baltic Sea at a rate of 3.4 ± 0.7 mm/year from 1993 to 2014, based on reconstructed tide gauge data, and a rate of 4.0 ± 1.3 mm/year from 1993 to 2015, utilizing satellite data.

In the area under study, the predominant coastal defense mechanisms, as determined by their proportion of the overall protected coastline, consist of dunes (40.9%) and dikes (17.5%), with seawalls and breakwaters being employed over relatively minor stretches. This heavy reliance on dunes marks a departure from the

coastal defense tactics observed along the German North Sea coast, where mainly three barrier islands (Sylt, Norderney, and Langeoog) are significantly augmented with approximately 1.8 million m³ of sand annually (see e.g. Staudt et al. (2021)). Dunes, serving as the principal form of coastal defense on the Baltic Sea, span roughly 106 km of the protected coastline (StALU, 2021). Nonetheless, these sand-based defenses are vulnerable to wave-induced erosion, especially during storm surge events. In areas facing a shortage of sediment, coastal management authorities engage in periodic dune nourishment to mitigate the risk of total dune erosion (StALU, 2021).

In addition to long-term trends, the impact of short-term sea level extremes, such as storm surges and wind waves, plays a crucial role in influencing coastal defense strategies (Suursaar et al., 2006; Madsen et al., 2015). In the Western Baltic Sea area, where the research is focused, storm surges typically rise to heights between 1.0 and 1.5 m, with surges over 1.0 m occurring between 1.2 and 2.1 times annually, varying by location (Weisse et al., 2021). Wave heights in the Baltic Sea exhibit a seasonal pattern, aligning with the winter's increased wind speeds (Björkqvist et al., 2018).

The studied coastal stretch lies in front of the village Ahrenshoop, situated at the Southwestern Baltic Sea close to the city of Rostock. The settlement lies on a land spit between the Baltic Sea and an inland lake (Bodden) known for its brackish waters. The strip of land here has a width of approx. 1000 m. It is protected by a 5.500 m long dune in combination with a 3.741 m long dyke, located behind the dune. Figure 2 illustrates an average beach profile, highlighting key measurements such as dune toe elevation, berm height, and the lowest low water level (LLWL). Additionally, a breakwater is located in the south of the study area and groynes are installed along the coast over the length of the dune. To the south of the dune there is a cliffed coast, while to the north, the flat coast continues into a nature protection area and ends in a sand spit (Darßer Ort). To protect the hinterland, the area north of the dunes is protected by a dike. The study area stretches over approximately 4 km and has a NE-SW orientation.

The transport directions of marine aggregates in the area are evident from other studies. Fröhle and Dimke (2008) evaluated the sediment transport directions and transport capacities using a numerical model called Genesis, which incorporates the widely used Coastal Engineering Research Centre (CERC) equation (Komar and Inman, 1970). For the studied area between Rostock and Zingst, they found transport capacities of up to 275 000 m³ per year, directed from the west to the east. They based their studies on the angle of wave attack, characteristics of the coastline, sediment characteristics, profile parameters, and structures.

The coastal region between Warnemünde and Ahrenshoop, facing NNW-WNW, is a fetch-limited coastline sheltered from waves originating from the Baltic Sea to the east. Kortekaas et al. (2010) utilized wave climate data recorded continuously over a five-year period (1998-2002) from a measuring station near Ahrenshoop. During this time, over 65% of the waves came from the W-WNW direction, with large storm waves typically arriving from WNW. The typical long-term wave conditions are summarized in Table 1 for five different load cases modelled by Kortekaas. Most commonly waves arrive at the beach with a significant wave height of 0.68 m and a period of 4.64 s and a direction of 276°. During 1-yearly storms, the direction stays the same while significant wave height and period increase to 1.29 m, respectively 5.77 s. In 5-yearly storms, the direction again stays the same though wave height increases to 1.4 m and the period increases to 6 s. Longer period swell waves were also simulated and came in from a direction of 347° with a significant wave height of 0.31m and a period of 6.09s. Additionally, Figure 3 provides a wave rose and water level series from a wave buoy at Ahrenshoop, showcasing the typical yearly variation in wave heights and water level. The coast here is regularly nourished every 3-6 years depending on the eroded volume of sand. Dunes are perceived as dynamic landforms subjected to erosion and deposition processes, necessitating regular maintenance to sustain their structural integrity. Since 1990, nine nourishments have been conducted ranging in volume from 15 221 m³ to 600 000 m³, while the mean volume amounts to approximately 350 000 m³ over an average length of 3 km. The typical volume of sand used for nourishment is 121 m³ per meter of coastline, while maintaining the dune and beach requires approximately 500,000 m³ of sand every 5 years. The nourishments counterbalance the continuing erosion of approximately 0.6 m/yr (StALU, 2021) eroded from the shoreline. The effect of a nourishment on neighboring locations and the interplay with the supply of sand from the cliff coast is important to optimize the use of sand. The supply of sand from marine sources is limited and complicated by the need to investigate the seabed for Unexploded Ordinance (UXO) and filter the dredged sand for UXO (Reckermann et al., 2022). Furthermore, animal and

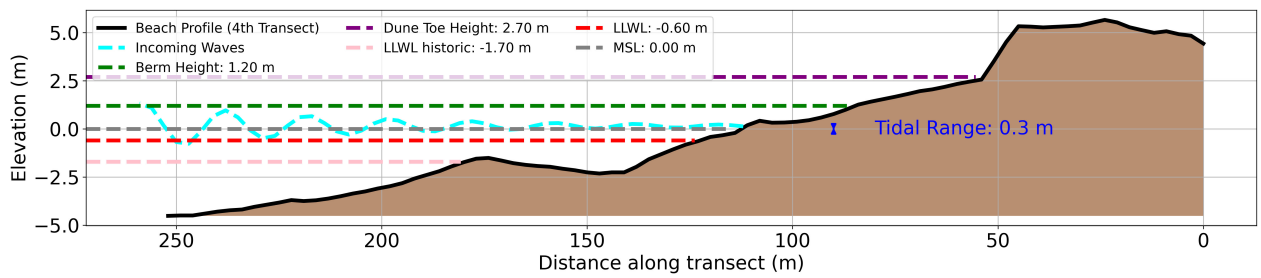

FIGURE 2
Average beach profile from transect 3 after nourishment. The sketch suggests wave breaking and shoaling through decreasing wave height, though it does not accurately depict these processes over the sandbar.

TABLE 1 Typical wave conditions for Ahrenshoop (Kortekaas et al., 2010).

Waves cases	Hs (m)	Tm (s)	Dir (°)
Local waves	0.68	4.64	276
Swell	0.31	6.09	347
Storm (1y)	1.29	5.77	276
Storm (5y)	1.40	6.00	276

nature protection concerns limit the areas where sand can be extracted.

Data collection and processing

Two data sources were exploited to evaluate the evolution of the nourishment project in Ahrenshoop. Subaqueous single-beam echo soundings cover the subaqueous part of the beach profile, while GPS measurements were used on the subaerial part. The data captures the progression of the nourishment from its inception through construction, as well as before and after its completion. This method, boasting high-frequency measurements and the capacity to encompass both terrestrial and subaqueous zones, facilitates a thorough assessment of the entire beach profile, spanning from the dune crest along the beach and foreshore profile up to a water depth of approximately 4.5 m.

The echo sounder and GPS surveying were commissioned by StALU MM to the surveying company Geogroup GmbH. The measurements were conducted using a Teledyne Reson E20 single beam and a Leica GPS. The accuracy of the system used for subaqueous measurements, as specified by the manufacturer, is ±2 cm ± 0.1% of the depth. For a maximum water depth of 10 meters, this results in an accuracy of approximately 3 cm. When accounting for the inaccuracy of the GPS, the total accuracy amounts to about 8 cm. Conversely, the subaerial measurements, which were conducted with a GPS probe, have an accuracy of 5 cm. Furthermore, the subaerial profile was monitored using an unmanned aerial vehicle (UAV), from October 2021 to November 2023. The UAV captured images that were processed using the photogrammetric software Metashape, resulting in the generation of digital surface models (DSM) and orthophotos. A summary of the measurement timeline is presented in Figure 4.

DSMs were acquired using UAV (DJI Phantom P4 RTK), which provides high-precision topographic data (Forlani et al., 2018). Typically, a standard UAV without a RTK receiver can only reproduce its precise location with an error margin of several meters, resulting in substantial errors. The planar accuracy is reliable within a few centimeters, while the vertical error can be far more substantial (Manfreda et al., 2019). To mitigate these inaccuracies, Ground Control Points (GCPs) can be deployed. GCPs are identifiable targets on the ground, surveyed with RTK GPS receivers, that are incorporated into the photogrammetric computation as fixed points, thereby generating DSMs with a precision of few centimeters (Štroner et al., 2020).

When using GCPs, attention must be given to their placement and flight parameters. UAV photogrammetry for beach leveling presents challenges due to difficulties in identifying common points in visually uniform areas. Jeong et al. (2018) showed that accuracy improves with lower flight altitudes, high image overlap, and a sufficient number of GCPs. Contreras-de-Villar et al. (2021) also emphasized that GCP placement, flight timing, and environmental conditions play a significant role in maintaining accuracy. High side overlap is crucial to prevent substantial increases in error rates when overlap is reduced.

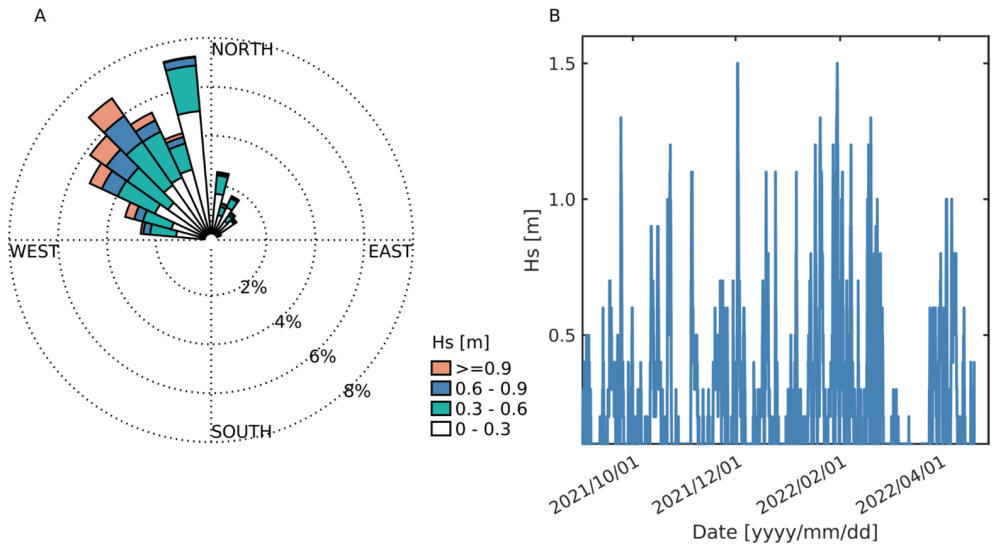

FIGURE 3
(A) Wave rose from a gauge at Ahrenshoop and **(B)** time series of water level fluctuations from a gauge in Warnemünde (adapted from Glueck and Schubert, 2024).

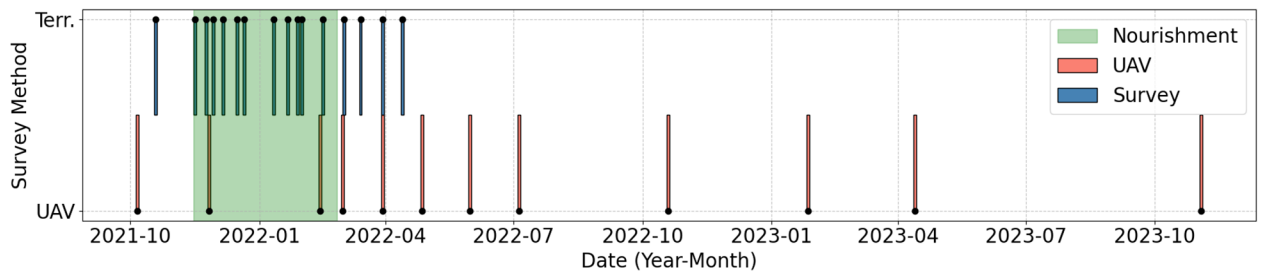

FIGURE 4
Timeline of the available complementary survey data. The surveys were conducted by a contractor at five transects inside the nourishment area. UAV: Photogrammetric surveys of the nourished area and adjacent beach segments. The green rectangle marks the period during which the nourishment was conducted.

Various studies highlight key factors affecting the vertical accuracy of digital elevation models (DEMs), digital terrain models (DTMs), and digital surface models (DSMs) derived from UAV imagery. Hugenholtz et al. (2013) found that the vertical accuracy of UAV-derived DTMs was comparable to LiDAR, with errors mainly due to vegetation. They suggest using LiDAR or minimizing vegetation in surveyed areas to improve accuracy. Gabara and Sawicki (2019) noted that increasing GCP density enhances vertical accuracy, but the benefits plateau beyond a certain threshold, recommending optimized GCP placement and UAV flight parameters. Contreras-de-Villar et al. (2021) observed that UAV-derived models' vertical accuracy is sensitive to environmental factors, recommending calm conditions and stable flight for better results. Fisher and Tate (2006) emphasized that robust interpolation techniques and error analysis are crucial for improving vertical accuracy in DEMs. Finally, Gindraux et al. (2017) highlighted the importance of GCP density and optimal flight parameters in achieving high vertical accuracy, especially in challenging terrains. Overall, these studies suggest careful planning and advanced techniques to enhance vertical accuracy across various applications.

However, in challenging or inaccessible terrains, using GCPs can be time-intensive and occasionally unfeasible. These issues can be mitigated by using RTK-enabled UAVs, which feature a build-in RTK enabled GPS receiver that can reproduce the location of the aircraft with an accuracy of a few centimeters (Štroner et al., 2021). This technology reduces reliance on GCPs for accurate positioning of the resulting DSMs. However, even with RTK enabled UAVs the vertical error can still amount to more than one meter (Nota et al., 2022), which can render the acquired DSMs not usable for change detection. To counter this, additional flights with an oblique camera angle can be used to reduce the vertical error (James and Robson, 2014).

An additional processing step that can enhance accuracy is a technique known as co-alignment. Cook and Dietze (2019) suggested that a high comparative accuracy between repeat UAV-surveys of the same study area can be achieved by aligning the images of different surveys together instead of processing them separately. After this alignment, the images are then divided by their respective survey date and processed further. This approach allows the forced alignment of poorly aligned surveys. A prerequisite for this to work is the presence of common elements in the surveys. In the case of the study at hand, common elements like the groins, infrastructure for access to the beach, or coastal view platforms make it suitable for this approach. As the groynes and coastal view platforms on the dune form the natural boundaries for the measured area, the alignments should be very reliable in contrast to a case where the only features available for alignment are in the center of the study area, leaving degrees of freedom open to the alignment process.

Nonetheless, Cook and Dietze (2019) cautioned that 3D models generated through co-alignment without GCPs might still contain absolute errors and distortions, such as doming (James and Robson, 2014; David et al., 2021). Furthermore, the absolute location accuracy of models created without GCPs is typically low, limiting comparisons with external sources like lidar topography (Neugirg, 2016).

We choose to use an RTK-enabled UAV for the image acquisition and incorporated oblique imagery as well as the so-called co-alignment in our workflow. The selection of flight and camera parameters was based on the methodologies outlined in the referenced literature. A detailed summary of these parameters, along with the corresponding accuracy achieved, is provided in Supplementary Table 1. After image acquisition Metashape was employed to process aerial images, generating high-resolution orthomosaics, DEMs, and 3D point clouds via the Structure-from-Motion (SfM) technique. Real-time kinematic GPS data was incorporated into the processing workflow to enhance spatial accuracy, resulting in horizontal accuracy within a few centimeters. However, vertical accuracy remained a challenge, with deviations of several decimeters. To address this, flight patterns were adjusted, introducing oblique imagery in March 2022 and conducting additional repeat flights utilizing 60° oblique camera angles from October 2022 onwards.

We employed four distinct processing workflows to compare their accuracy (Figure 5). The first two workflows utilized direct georeferencing from the RTK UAV: one using only nadir images and the other incorporating both nadir and oblique images. The remaining two workflows followed a co-alignment approach: one using only nadir images and the other incorporating both nadir and oblique images, where all images were initially aligned together and then segmented into the respective surveys.

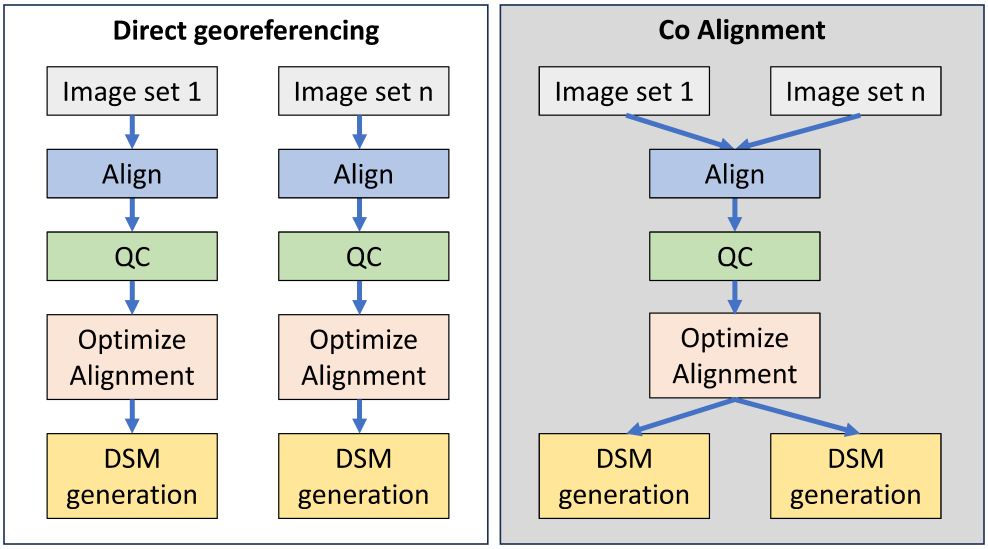

FIGURE 5
Different workflow processes in Metashape. DSM generation consists of building the dense point cloud and computing DSMs and orthophotos from it. The resulting models (digital surface models) capture the Earth's surface elevations, including all structures and vegetation.

Volumetric change

We conducted a comprehensive analysis to examine sediment volume changes following nourishment efforts. Utilizing the survey data spanning from October 2021 to March 2022, covering the nourishment construction period, and UAV data extending from October 2021 to November 2023, encompassing the post-nourishment period, we scrutinized profiles along each of the five transects within the project area. The transects are distributed over the study area and displayed in Figure 1B. The transects in this study were spaced at an average distance of 650 meters, a spacing determined by logistical constraints but recognized as a potential source of significant error in volumetric calculations. This wide spacing raises concerns about the accuracy of estimating beach-wide volumetric changes, as it is likely to miss critical morphological features that exist between the widely spaced transects. According to the findings of Muñoz-Pérez et al. (2012), errors in volumetric estimation increase substantially as transect spacing widens, particularly beyond 300 meters. With a spacing of 650 meters, the error in estimating total volumetric changes across the entire beach could exceed 100%. This high error margin stems from the likelihood that significant profile variations—such as dunes, erosional features, or other critical changes—are not captured, leading to substantial under- or over-estimations of the beach's volume.

Given these limitations, the methodology applied here focuses on estimating volumetric changes within each individual transect, rather than attempting to extrapolate these measurements to represent the entire beach. While this approach reduces some of the potential error introduced by wide spacing, it is important to acknowledge that any broader generalizations based on these transect-specific estimates are likely to be unreliable. The conclusions drawn from these volumetric calculations should, therefore, be treated with caution, especially when considering the beach as a whole. Further refinement of the methodology, possibly through additional data collection or alternative analytical techniques, would be necessary to achieve more accurate and reliable volumetric estimates across the entire beach.

Subsequently, we applied a straightforward volume calculation method to measure alterations in sediment volume between adjacent profiles. To evaluate the volume change, we applied the trapezoidal rule to integrate the areas between consecutive beach profiles. For a single interval, the trapezoidal rule is expressed as:

$$\int_a^b f(x)dx \sim \frac{b-a}{2}[f(a)+f(b)]$$

Uncertainty estimation

The data collected from both terrestrial and UAV measurements inherently carries a degree of uncertainty due to the errors of the sensors and computation themselves and also the GPS accuracy. Additionally, the process of computing volumes introduces further uncertainty, which compounds as the measurement error propagates through the trapezoidal integration method. The integration with the trapezoidal rule introduces an error to the computed volumes as the curves of the beach profiles can only be approximated by the straight lines in the trapezoid. However, if the interval between adjacent points is small enough the error can be kept to a minimum. The measurement uncertainty for terrestrial monitoring, provided by the device manufacturer and the surveying company, was 0.08 m, while the uncertainty for UAV-based measurements, derived from our own analysis, was 0.14 m. Although these values are conservative and, in some cases, may be much better, they were chosen to ensure a robust assessment of the validity of the results. We computed the

combined error and give an error estimate for the volumes and changes for each of the measurement systems.

The uncertainty due to the measurement error is given as:

$$\sigma_{Meas} = \Delta y * \Delta x * \sqrt{n}$$

Where Δx =(b−a) is the distance between the measurement stations, Δy is the measurement error, and n is the number of subintervals.

The error due to the approximation of the curves by straight lines in the trapezoids is given by Cheney and Kincaid (1998) as:

$$E_{Trapez} = \frac{(b-a)^3}{12n^2} f''(\xi)$$

Where n is the number of subintervals, ξ is the point in the interval an f′′(ξ) is the second derivative of f(x) evaluated at ξ.

To reduce the error introduced by the trapezoidal integration, we applied cubic interpolation to the 3 m resolution transects, refining them to a 0.5 m resolution. This approach improved the accuracy of the volume calculations. Further increasing the resolution beyond 0.5 m did not result in significant changes to the computed volumes, leading us to select 0.5 m as the optimal resolution for this analysis.

To estimate the uncertainty in the volume assessments, the individual sources of uncertainty, including measurement and trapezoidal rule errors, are combined. These uncertainties are summed using the quadrature method, which accounts for the independent contributions of each uncertainty source (Lane et al., 2003; Wheaton et al., 2010):

$$\sigma_{total} = \sqrt{\sigma_{Meas}^2 + E_{Trapez}^2}$$

Then the cumulative uncertainty in volume change for each transects is propagated across the surveys using a quadrature sum of the uncertainties in each time step:

$$\boldsymbol{\sigma} = \sqrt{\sum_{i=1}^{n} \boldsymbol{\sigma}_{total,i}^2}$$

Drivers

To assess the underlying drivers and impacts leading to documented morphological changes on site, we coupled the erosion and deposition trends of the nourishment to data from a wave buoy off the coast. As the main drivers, we calculated the cumulative wave energy between the survey time steps, total water level, including the wave runup, and wave direction.

The wave parameters were obtained from two offshore wave buoys, FINO2 and Arkona, operated by the Federal Maritime and Hydrographic Agency (BSH). The buoys lie approximately 40 km offshore of the beach and deliver quality-controlled *in situ* wave parameters, which is available from the BSH open Data portal (BSH - Seegang, 2024).

From this data, the total water level (TWL) was calculated using the equation by Sallenger (2000) as:

$$TWL = \eta + R_{2\%}$$

With η being the mean sea level (MSL) and $R_{2\%}$ being the wave runup. The data for η was obtained from water gauge measurements at the closest gauge in Warnemünde, located at a distance of 25 km from Ahrenshoop. For the wave runup, we used the approach outlined by Stockdon et al. (2006). Their approach relies on offshore wave buoys to provide significant wave height and wave period. Using these offshore wave conditions, their empirical equation predicts the wave runup height on sandy shorelines. The beach slope at Ahrenshoop is initially 0.04 [-] following nourishment and gradually steepens to approximately 0.08 [-] over the course of the three-month survey period. According to the widely accepted Iribarren Number (Battjes, 1974), this places Ahrenshoop at the boundary between a dissipative and an intermediate beach, with the potential to become fully reflective as the slope increases. Given that the beach slope is expected to exceed 0.04, we have chosen to use a higher slope value in our calculations to avoid underestimating wave runup. Additionally, the equilibrium beach profile was determined. After a nourishment, the artificially crafted beach profile is usually too steep and far from mimicking a sort of natural profile. Over the course of days and weeks, the forcing by waves redistributes the sand volumes to form a gentler profile that reflects less of the waves and changes the beach towards a more dissipative characteristic. This profile is called the equilibrium profile and it is commonly estimated from the equations as given by Bruun-Dean (Bruun, 1954; Dean, 1977):

$$h = Ax^{2/3}$$

The parameter A refers to the so-called profile scale that can be estimated from the sediment size. The parameter signifies the steepness of the profile. The variables x and h represent the horizontal distance and height along the profile, respectively. For the Baltic Sea with a mean grain size of d_{50} = 0.33 mm the parameter A is given by Dean (1987) as follows:

$$A = 0.41 * {d_{50}}^{0.94}$$

Additionally, the wave energy per unit area was calculated using the significant wave height (Hs) following the methodology outlined by Holthuijsen (2007). The wave energy (E) was computed using the equation:

$$E = \frac{1}{8} * \rho * g * Hs^2$$

Where E is the wave energy (J/m²), ρ is the density of seawater in the Baltic Sea (1005 kg/m³) (Feistel et al., 2010), g is the acceleration due to gravity (9.81 m/s²), and Hs the significant wave height.

Results

Accuracy assessment of UAV photogrammetry

We used stable areas for calculating the accuracy of the DSMs. Three validation points were identified, each corresponding to the southern, northern, and central parts of the study area (Figure 6). The evaluation of direct georeferencing performance revealed substantial variability in vertical accuracy, which is inadequate for most precision-dependent applications. The results show that the standard deviation of vertical accuracy for direct georeferencing without oblique imagery was measured at 0.25 m, 0.24 m, and 0.23 m in the South, Mid, and North, respectively. Additionally, the maximal differences in these regions were 0.64 m, 0.66 m, and 0.66 m, respectively, indicating considerable inconsistency in the elevation data. This variability poses a significant challenge for applications requiring high accuracy, such as detailed topographical mapping and precise construction projects.

The introduction of oblique imagery to the direct georeferencing workflow, which was anticipated to enhance the vertical accuracy, did not yield the expected improvements. On the contrary, the inclusion of oblique images resulted in a deterioration of accuracy. The standard deviations increased to 0.29 m, 0.32 m, and 0.35 m in the South, Mid and North, respectively. Similarly, the maximal differences escalated to 1.01 m, 1.12 m, and 1.26 m in the respective regions. This decline suggests that simply adding oblique imagery to direct georeferencing, without additional corrective measures, may introduce errors that exacerbate the variability rather than reduce it. We speculate that the different lighting conditions during the repeat flight offset the accuracy of the photogrammetric reconstructing.

In response to the limitations observed with direct georeferencing, a co-alignment step was incorporated into the data processing workflow. This adjustment significantly enhanced the vertical accuracy, bringing about nearly an order of magnitude improvement in the standard deviation, which was reduced to 0.04 m across all surveyed regions, with corresponding maximal differences of 0.11 m, 0.12 m, and 0.16 m in the South, Mid, and North, respectively. This considerable improvement highlights the efficacy of the co-alignment step in correcting the inaccuracies and inconsistencies inherent in direct georeferencing methods. The co-alignment process likely aids in refining the alignment of imagery, thereby reducing discrepancies and enhancing the overall fidelity of the elevation data.

Further refinement was pursued by integrating oblique imagery into the co-alignment workflow, a strategy aimed at leveraging the additional perspective provided by oblique views to enhance vertical accuracy further. This integration resulted in a noteworthy reduction in the standard deviation to 0.02 m, 0.03 m, and 0.05 m in the South, Mid and North, respectively, surpassing the improvements achieved by co-alignment alone. The maximal differences were concurrently reduced to 0.06 m, 0.14 m, and 0.12 m in the South, Mid, and North, respectively. These results underscore the benefit of combining oblique imagery with co-alignment, as the additional perspectives obtained from oblique angles appear to facilitate a more precise alignment and correction process, thereby delivering superior vertical accuracy. The results of the different workflows are displayed in Figure 7.

Morphological development during the nourishment

Profile changes

Figure 8 illustrates the locations of the transects, which are incrementally numbered from southeast to northwest,

FIGURE 6
(A) Overview of study area, **(B)** Check point South, **(C)** Check point Mid, **(D)** Check point North. Background Panel **(A)** Bing Satellite.

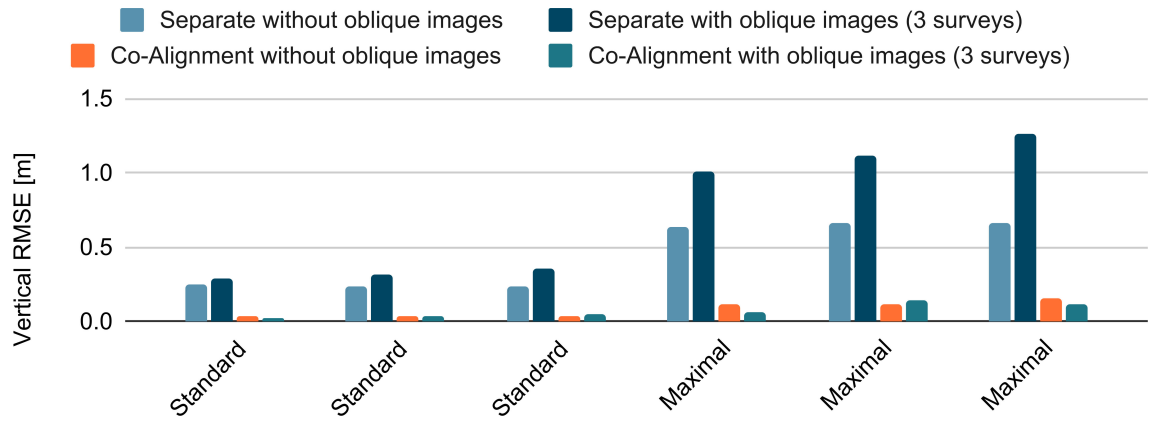

FIGURE 7
Bar plots illustrating the performance of four workflows across three check points, as depicted in Figure 6. The workflows include separate processing with and without oblique images, co-alignment with and without oblique images. The oblique images, acquired for three surveys, were incorporated into the respective processing workflows. Performance metrics are presented by the standard deviation and maximum differences calculated across surveys.

corresponding to the direction of net sediment transport. Each transect is approx. 250 m in length, encompassing the dune, beach, and foreshore, extending to a depth of approx. 4.5 m below MSL. To the south of the study area, a breakwater restricts longshore sediment transport. Further south, the coastline transitions to a cliffed coast. Notably, the shoreline angle relative to the wave direction becomes steeper moving northward, with a significant directional change occurring between transects 2 and 3. All transects, except for transect 5, are located in areas equipped with groynes. The satellite imagery reveals a system of two sandbars extending across most of the transects, with notable switching episodes between transects 2 and 3, where the inner and outer bars switch positions or merge to form a single bar.

Figure 9 presents a comprehensive overview of the outcomes derived from terrestrial-monitoring efforts. The measured elevations range from approximately -4 to 5.5 m, encapsulating the subaqueous beach profile up to the forefront of the dune system. Across various transects, discernible responses to both nourishment initiatives and metocean influences are observed. Transects 1 and 2, being more sheltered due to their directional orientation, exhibit minor dune recession, concurrent with erosion affecting the beach and foreshore regions. In transect 1, a nourishment of 77.32 m^3/m was conducted. Following the nourishment, a positive change of 10.50 ± 0.63 m^3/m was observed. The process has led to the formation of a solitary sandbar, while transect 2, which received 47.55 m^3/m of nourishment, experienced a negative change of -15.78 ± 0.87 m^3/m after the nourishment, along with the emergence of two distinct sandbars.

In contrast, transects 3 through 5, being more exposed, experience more distinct responses compared to transects 1 and 2. Transect 3 experiences moderate dune accretion and corresponding beach erosion, with minor foreshore erosion. A total nourishment of 76.66 m^3/m was carried out, resulting in a positive change of 3.95 ± 0.31 m^3/m. Notably, the pre-existing sandbar undergoes offshore migration while concurrently augmenting in elevation. Transect 4 shows minimal dune and beach erosion, juxtaposed with strong foreshore accretion, following a nourishment of 54.49 m^3/m. Post-nourishment observations revealed a positive change of 23.27 ± 0.70 m^3/m. The seaward displacement of the existent sandbar leads to the development of a terrace. The resulting profile looks very similar to the pre-nourishment profile, though moved further seaward.

In all transects besides 5, the presence of groynes is noted, contributing to localized variations in sediment dynamics and

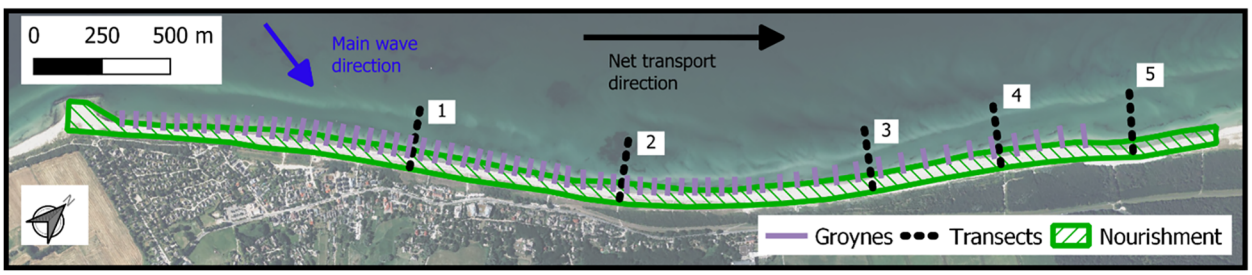

FIGURE 8
Overview map of the transects. Transect 1 is located close to the breakwater, while transect 5 marks the transition to the adjacent national park. Note the absence of groynes in transect 5. Background: Bing Satellite.

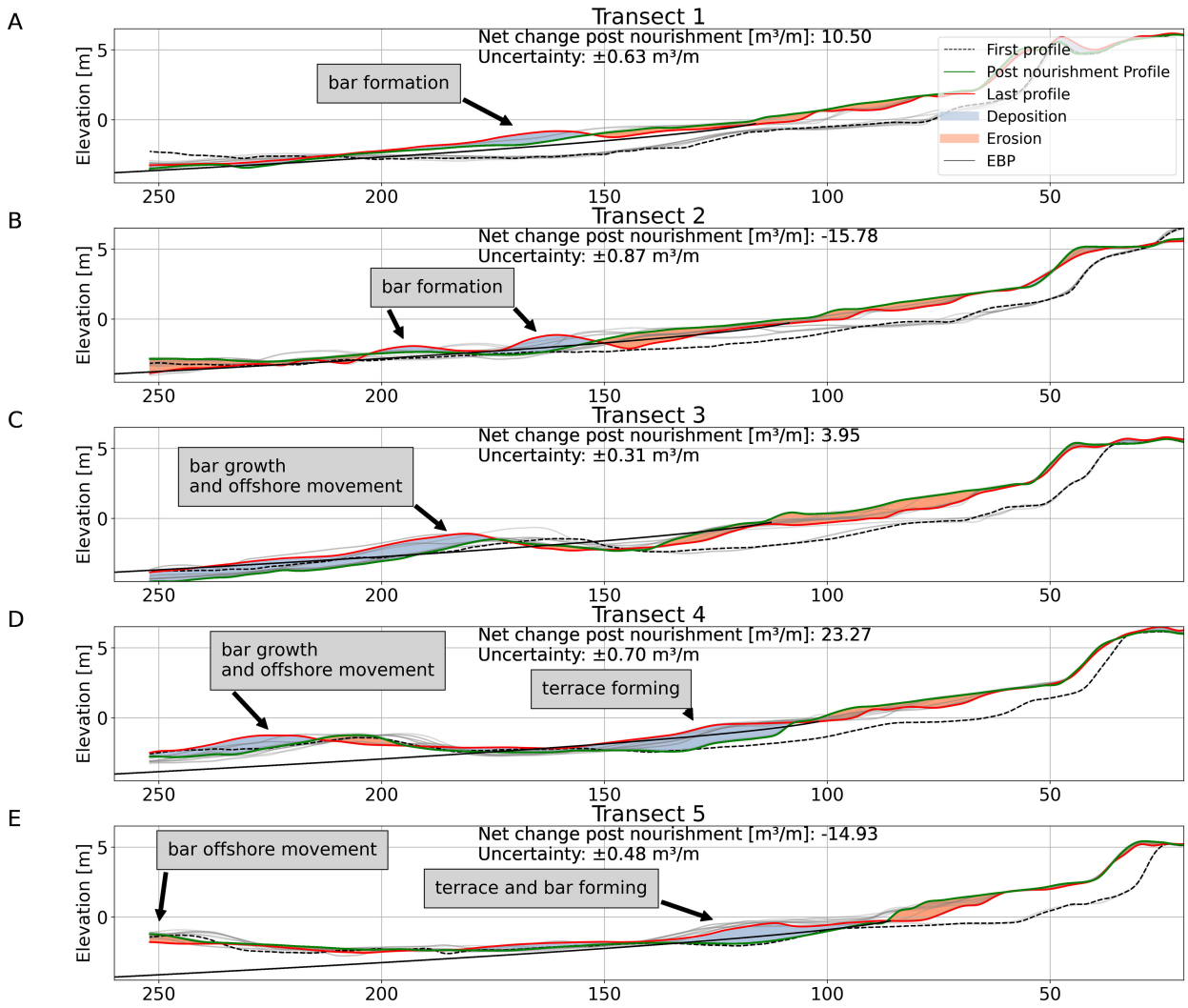

FIGURE 9
Beach profiles of the five transects (labeled as panel **A–E**). The first measured profiles before the beginning of the nourishment are marked in dashed black lines, the post-nourishment profiles are plotted in green, while the last measured profiles are plotted in orange. The shaded areas indicate the changes in sand volume between the post-nourishment profile (green) and the last measured profile (orange), with orange representing erosion and blue indicating deposition across each transect.

coastal morphodynamics. Transect 5 showcases limited dune erosion but pronounced beach erosion, coupled with strong foreshore accretion. Despite receiving a total nourishment of 75.58 m^3/m, a negative change of -14.93 ± 0.48 m^3/m was observed. In the foreshore, a longshore bar seems to develop, though very small in height in the measured timeframe. Notably, indications within the profile hint at the offshore migration of the existing offshore sandbar, although the bar seemed to have moved into uncharted territory in the last time steps. This also explains why the fifth profile experiences a negative change after nourishment. Note that the uncertainty in these volume changes is given as the propagated error between the two time steps that are being compared and is therefore lower than the propagated error when including all time steps.

All the transects experience either the emergence of bars in previously unbarred profiles or if existing bars were present, their offshore movement and vertical growth after the nourishment. An extrapolation into the future seems to suggest that transects 4 and 5 are on the verge of developing a new bar close to the shore. In transect 5 the bar at the end of the terrace is already showing a small indentation. The bars in transects 4 to 5 seem to mitigate erosion in the nearshore area by inducing wave breaking and allowing a terrace to form. Table 2 provides a detailed summary of the characteristics observed across each transect, including time since nourishment, bar formation and movement, offshore bar distance, and patterns of erosion or accretion on the terrace and beach.

Beach slope

Figure 10 shows a line plot (A) and a heatmap (B) of the beach slope development in each transect over time. Each transect starts out with a fairly gentle slope of 0.08 to 0.1 [-]. Transect 4 stands out with the highest beach slope of approx. 0.1 [-]. The impact of the

TABLE 2 Characteristics of each transect post-nourishment, detailing time since nourishment, bar formation and movement, bar distance offshore, and observed erosion or accretion on the terrace and beach.

T. no.	Time since nourishment in month	Existing bar	Bar formation	Bar movement	Bar distance	Terrace	Beach
1	2,5	No	1 bar	No	60	Erosion	Erosion
2	3	No	2 bars	No	75, 105	Strong erosion	Strong erosion
3	4	Yes	No	Offshore	95	Erosion	Strong erosion
4	5	Yes	No	Offshore	135	Accretion	Erosion
5	4,5	Yes	1 bar (nearshore)	Offshore	175	Accretion	Erosion

nourishment is clearly visible in each transect, manifesting in a strong decrease of the steepness to a value of approx. 0.04 [-]. After nourishment, all transects generally show a trend towards a steeper beach slope. Transects 3 and 5 notably reach their initial steepness approximately 3.5 and 4 months after nourishment, respectively.

Bar migration

The migration of sandbars in transects 3 and 5 follows well-established mechanisms where large waves cause offshore sediment movement. When large waves break over the sandbar, they generate strong offshore-directed currents near the bar crest, pushing sediment seaward (Wright and Short, 1984; Leont'ev, 2011). In contrast, during calmer conditions with smaller waves, sandbars migrate shoreward as the waves shoal without breaking, creating onshore-directed forces that transport sediment landward, especially near the crest (Quartel et al., 2008). The position of the sandbar and the TWL also play critical roles, as higher TWL during storms allows more wave energy to pass over the bar, potentially causing overwash and increasing erosion (Fontán-Bouzas et al., 2022).

The location of sandbars for transects 3 (red) and 4 (blue) fluctuates significantly (Figure 11A). During high wave energy periods, such as at the end of January and the end of February 2022, there are notable changes in bar location. For instance, transect 3 exhibits considerable movement during these peaks, indicating that strong wave action displaces the sandbar offshore. Conversely, during periods of lower wave energy, such as in the middle of February 2022, the bar moves further onshore by approx. 2 m in transect 4 and 1 m in transect 3. In general, reduced wave action allows the sandbars to remain stationary with only minor adjustments in position.

The height of the bar crest for both transects exhibits variations influenced by wave energy. During high-energy wave events, such as those observed in January and February 2022, significant changes in bar crest height occur (Figure 11B). For instance, at the end of January 2022, the crest height of the bar in transects 3 and 4 decreased markedly by 0.25 m in transect 3 and 0.5 m in transect 4. Additionally, the bar shifted offshore by 3 m in transect 3 and 4 meters in transect 4. In the calmer period in the first half of February, the bar in transect 3 grew in height by more than 1 m, while the bar in transect 4 recovered to its pre-storm height of 1.2 m. The following storm at the end of February 2022 decreases the height of the bar crest in transect 3 again to pre-storm levels, though the bar crest height in transect 4 only slightly decreases.

The two storms appear to force the morphology of the beach profile with similar levels of wave energy, though a marked difference between the characteristics of the two storms lies in the TWL (Figure 11C). A specific feature of the Baltic Sea is the coincident occurrence of low water due to the water being pushed out of the basin by the wind and storm waves. This behavior is evident at the end of January 2022 (Figure 11C), where the combination of these two phenomena causes the most significant decrease in the height of the sand bar in transects 3 and 4. Other storm events are not able to change the bar position and height in such a manner.

During periods of lower wave energy, such as December 2021 and March 2022, the bar crest height tends to stabilize or exhibit gradual changes. These conditions promote sediment deposition and accumulation, resulting in a slow but steady increase in crest height. During periods of increasing bar crest height, the bar location shifts onshore, whereas, during periods of decreasing bar crest height, it moves offshore.

Notably, the profiles in adjacent transects 1 and 2 behave similarly to transect 4 in terms of beach slope development but differ from transect 3 (Figure 11D). Transects 1 and 2 share the same orientation, as do transects 3 and 4. Consequently, the incident direction of the waves does not appear to be the deciding factor. The differing bar heights could be related to the switching periods in the sand bars observed in satellite images. Bar switching behavior is not entirely understood but is linked to alongshore differences in the position and depth of the outer bar (Shand, 2003).

Volumetric change

Figure 12 illustrates the volumetric changes across each transect. The most significant alterations to the subaerial section of the profile can be attributed to the nourishment process. Each profile exhibits a substantial increase in volume up to February 2022, when nourishment is completed. Thereafter, all transects develop in a similar pattern. Notably, after an initial significant variation in changes over the time steps, the cumulative volume trends converge for all transects. The bottom panel shows the changes occurring below MSL to a depth of approximately 4 m. Alterations in the subaerial section partially align with changes in

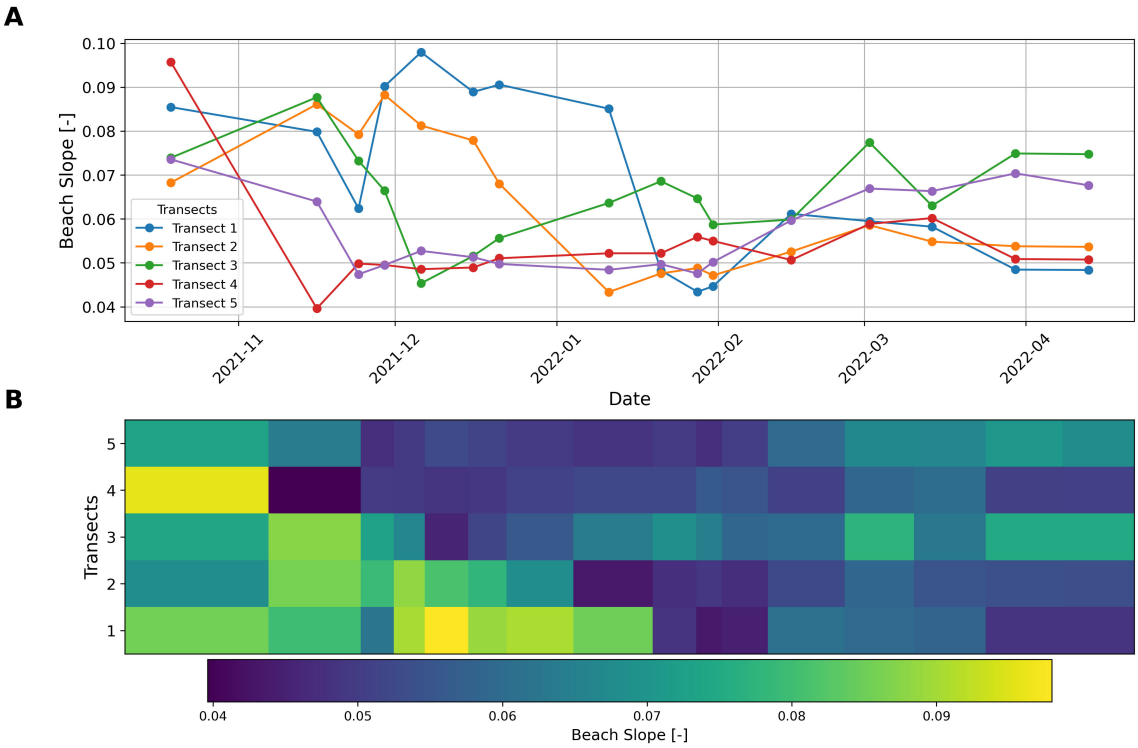

FIGURE 10
The development of the beach slope (between 0 m and 2.5 m above MSL) in each transect over time. Depicted as a lineplot in **(A)** and a heatmap in **(B)**.

the subaqueous portion. For instance, nourishment in transect 3 enhances the volume across all subaqueous transects. The subaqueous transects correlate with nourishment in the subaerial transects, which is particularly evident in transect 1, where subaqueous volume markedly increases following nourishment in that transect. In the final few time steps, beginning in mid-February, subaqueous volume decreases in transects 2 and 5, while the other three transects show an increase in volume.

These underwater changes are closely related to low water levels, as the subaqueous profile becomes more exposed to wave action, which intensifies erosion. This is highlighted by historical sea level data for Warnemünde, where the most extreme Lowest Low Water Level (LLWL) of -170 cm below MSL was recorded on October 18, 1967 (Wolski et al., 2014). During the monitoring of the beach profile, the LLWL observed was -0.59 m below MSL on the 19.02.2022, followed by low water of -0.38 m below MSL on 21.02.2022.

In transect 1, located to the south, a nourishment of 77.32 m^3 per meter was conducted. After nourishment, the net change was a loss of 2.36 m^3 per meter above MSL, while below MSL, transect 1 experienced a gain of 12.86 m^3 per meter. The combined net change for transect 1 is a total gain of 10.50 m^3 per meter. The presence of a breakwater near transect 1 limits the across-shore sediment transport that would typically replenish this area, particularly above MSL. Moving northward to transect 2, which received 47.55 m^3 per meter of nourishment, the net volume change was a loss of 8.31 m^3 per meter above MSL, coupled with a loss of 7.47 m^3 per meter below MSL. The combined net change for transect 2 is a total loss of 15.78 m^3 per meter. This transect shows a decrease in sediment volume both above and below MSL, with significant losses overall. In transect 3, further north, a nourishment of 76.66 m^3 per meter was carried out. Above MSL, the transect experienced a net loss of 8.88 m^3 per meter, while below MSL, transect 3 showed a gain of 12.83 m^3 per meter, leading to a combined net gain of 3.95 m^3 per meter. Transect 4, positioned further north, received 54.49 m^3 per meter of nourishment. It exhibited a net loss of 3.29 m^3 per meter above MSL and a gain of 26.56 m^3 per meter below MSL. The combined net change for transect 4 is a total gain of 23.27 m^3 per meter, representing a significant positive change. Finally, transect 5, the northernmost transect, was nourished with 75.58 m^3 per meter. After nourishment, it showed a net loss of 6.74 m^3 per meter above MSL, while below MSL, transect 5 recorded a gain of 8.17 m^3 per meter, resulting in a combined net loss of 14.90 m^3 per meter.

In summary, the data reveals a consistent pattern of sediment loss above MSL across all transects, while below MSL, the transects generally show positive changes, particularly in the more northern areas. The presence of the breakwater near transect 1 influences the sediment dynamics, limiting sediment supply to the southern transects, contributing to the observed patterns of erosion and deposition along the beach profiles.

Medium-term monitoring

Medium-term monitoring of the coastal transects reveals distinct patterns in erosion rates and the effectiveness of sand nourishments (Figure 13). Transects 1 and 2 exhibited the highest erosion rates on the beach and dune. Following the completion of the nourishment

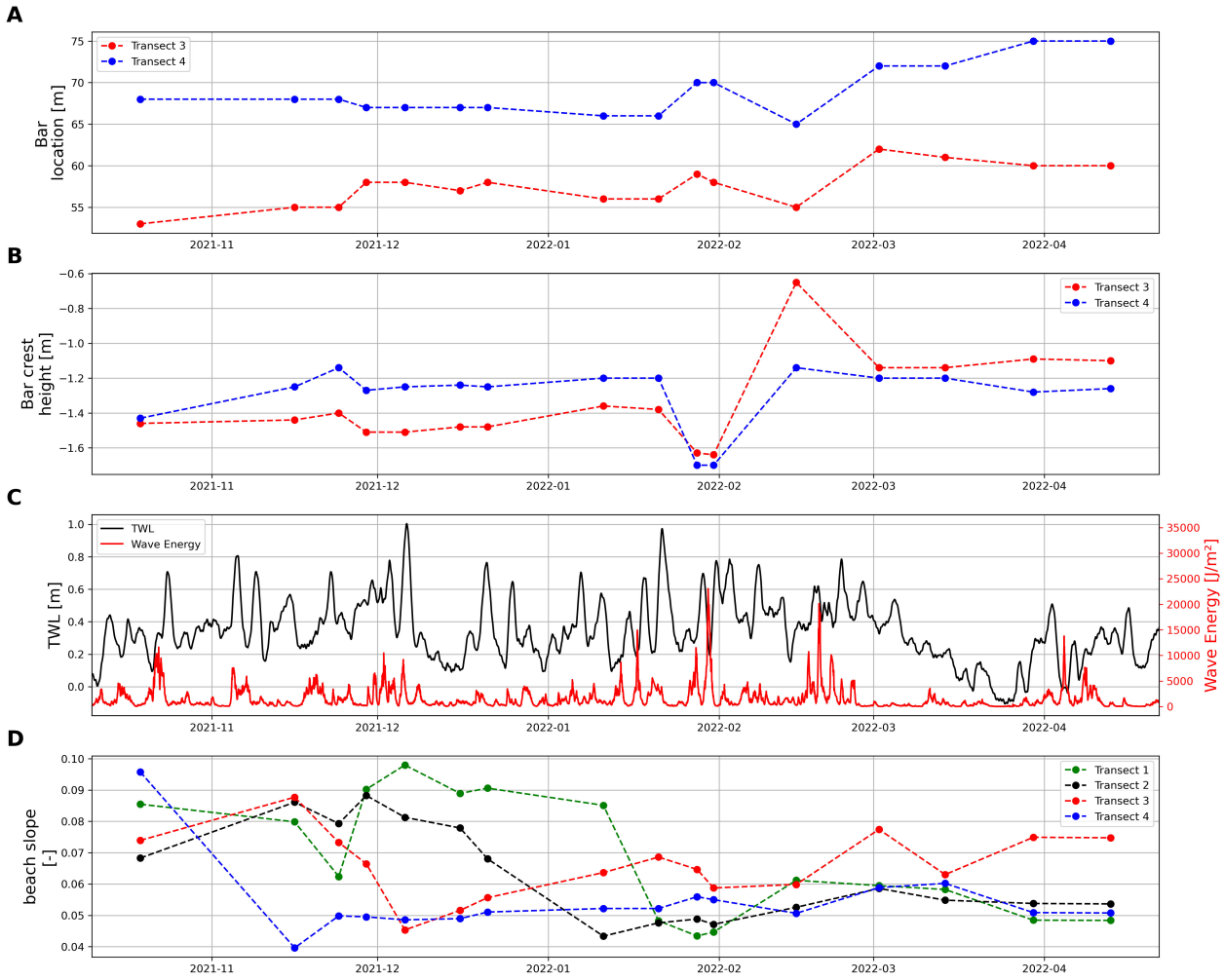

FIGURE 11
Parameters describing the bar processes driving and influencing the bar morphology in transects 3 and 4. **(A)** distance of the bar location to the shoreline at MSL, **(B)** bar crest height, **(C)** TWL (sum of sea level and wave runup) and wave energy, **(D)** beach slope.

project, the volume per meter decreased by 17.58 m^3/m and 12.04 m^3/m, respectively. These significant decreases suggest that the sandbars generated during the nourishment were ineffective in providing adequate protection against wave energy. As a result, these transects experienced considerable erosion, indicating that the protective function of the newly formed sandbars was suboptimal.

In contrast, transects 3 and 4 experienced minimal erosion rates, with volumetric changes of -6.94 m^3/m and -4.24 m^3/m, respectively. The presence of existing offshore sandbars, which increased in height and distance from the shore after the nourishment, provided substantial protection. These sandbars effectively dissipated wave energy, causing the waves to break before reaching the beach and dune. This pre-breaking of waves reduced the energy impacting the shore, thus minimizing erosion and demonstrating the protective benefits of well-positioned offshore sandbars.

Transect 5 showed a significant erosion rate of 7.49 m^3/m. This suggests that the associated offshore sandbar was positioned too far from the shore. Although the sandbar induced initial wave breaking, the waves seemingly had enough distance to reform and regain energy before impacting the beach and dune. This re-energization of waves between the offshore sandbar and the shoreline likely contributed to the observed erosion at transect 5.

The differential performance of the transects underscores the critical importance of optimal sandbar positioning in coastal nourishment projects. Transects 1 and 2, with less effective nearshore sandbars, exhibited higher erosion rates, whereas transects 3 and 4 benefited from strategically positioned offshore sandbars that provided significant protection. However, it must be noted that the cross-shore transport in the region is directed from transect 1 to transect 5, indicating that cross-shore processes could also contribute to the lower erosion rates observed towards transect 5. The situation at transect 5 highlights a crucial consideration in nourishment design: sandbars located too far offshore may fail to protect the coast adequately due to wave reformation.

Discussion

Sandbars are essential for coastal protection, as they dissipate wave energy before it reaches the shore. However, if sandbars are

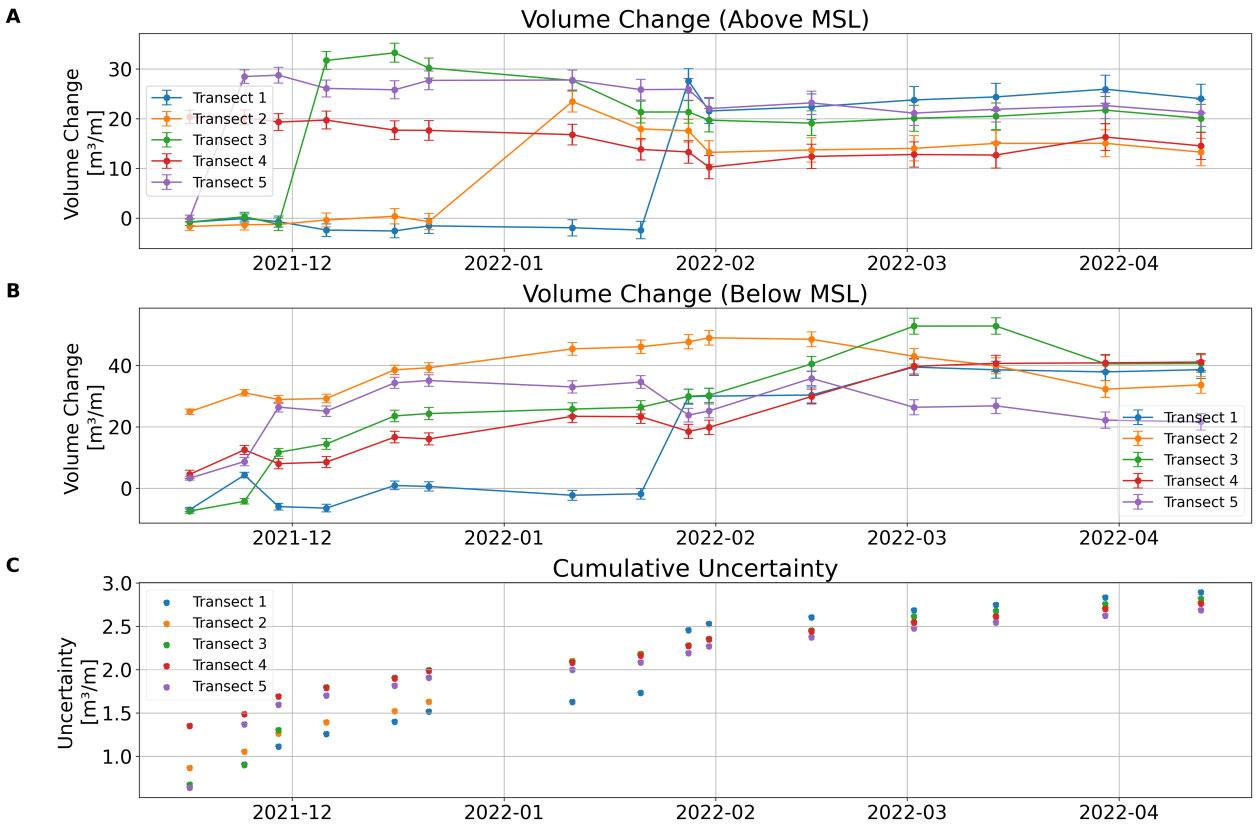

FIGURE 12
Volumetric change above MSL **(A)**, below MSL **(B)**, and cumulative uncertainty **(C)**. Errorbars mark the cumulative uncertainty in **(A, B)**. Depicted is the volumetric change in each transect.

located too far offshore, waves may reform and break on the beach, reducing the protective effect. The impact of sand nourishments on the development of subaqueous sandbars and their interactions with coastal processes remains relatively understudied. This gap persists despite using advanced monitoring systems such as subaqueous echo sounding and UAVs. The complexity arises from the diverse range of sand nourishment techniques, variability in coastal metocean conditions, and the heterogeneous nature of coastal environments.

de Schipper et al. (2016) investigated the initial response of the Sand Engine, a major nourishment project that used 21 million m^3 of sand. They observed the formation, vertical growth, and downslope migration of a subtidal sandbar within months of construction, with the sandbar forming approximately 300 m offshore. In our study at Ahrenshoop, we observed similar phenomena but with notable differences. The newly formed sandbar at Ahrenshoop was much closer to the shoreline, approximately 60 m offshore, compared to the Sand Engine's 300 m. Additionally, the metocean conditions in the Baltic Sea at Ahrenshoop, which lack significant tidal influence, differ markedly from the tidal conditions of the North Sea at the Sand Engine. This difference in conditions influenced the formation and evolution of the sandbars. Before nourishment, Ahrenshoop had a non-barred profile, unlike the barred profile observed at the Sand Engine site.

Along transect 2 the nourishment led to the formation of multiple sandbars, with two prominent bars emerging at distances of 75 m and 105 m from the shoreline. These bars were sustained by the erosion of the beach below a height of 1.0 m and the subtidal terrace.

Comparing our findings with Radermacher et al. (2018), several key differences and similarities emerge. Radermacher et al. (2018) found that beach nourishments typically lead to subtidal sandbar formation within three years, while shoreface nourishments result in rapid onshore migration of sandbars at rates of 20-60 m/year, often causing pre-existing sandbars to merge with the beach. Mega-nourishments, such as the Sand Engine, induced the formation of new, shallow sandbars with significant alongshore variability. Our study corroborates some of these findings but highlights faster sandbar formation within two months and their closer proximity to the shore. These differences likely stem from the differing metocean conditions and nourishment techniques employed.

Gijsman et al. (2021) observed significant and systematic alongshore differences in sandbar geometry along the curved coastline of Sylt, with the northern half featuring less pronounced sandbars closer to the shoreline and the southern half displaying more pronounced sandbars further offshore. The coastline at Ahrenshoop is also curved, though it is concave rather than convex as seen on Sylt. In our observations, sandbars are closer to

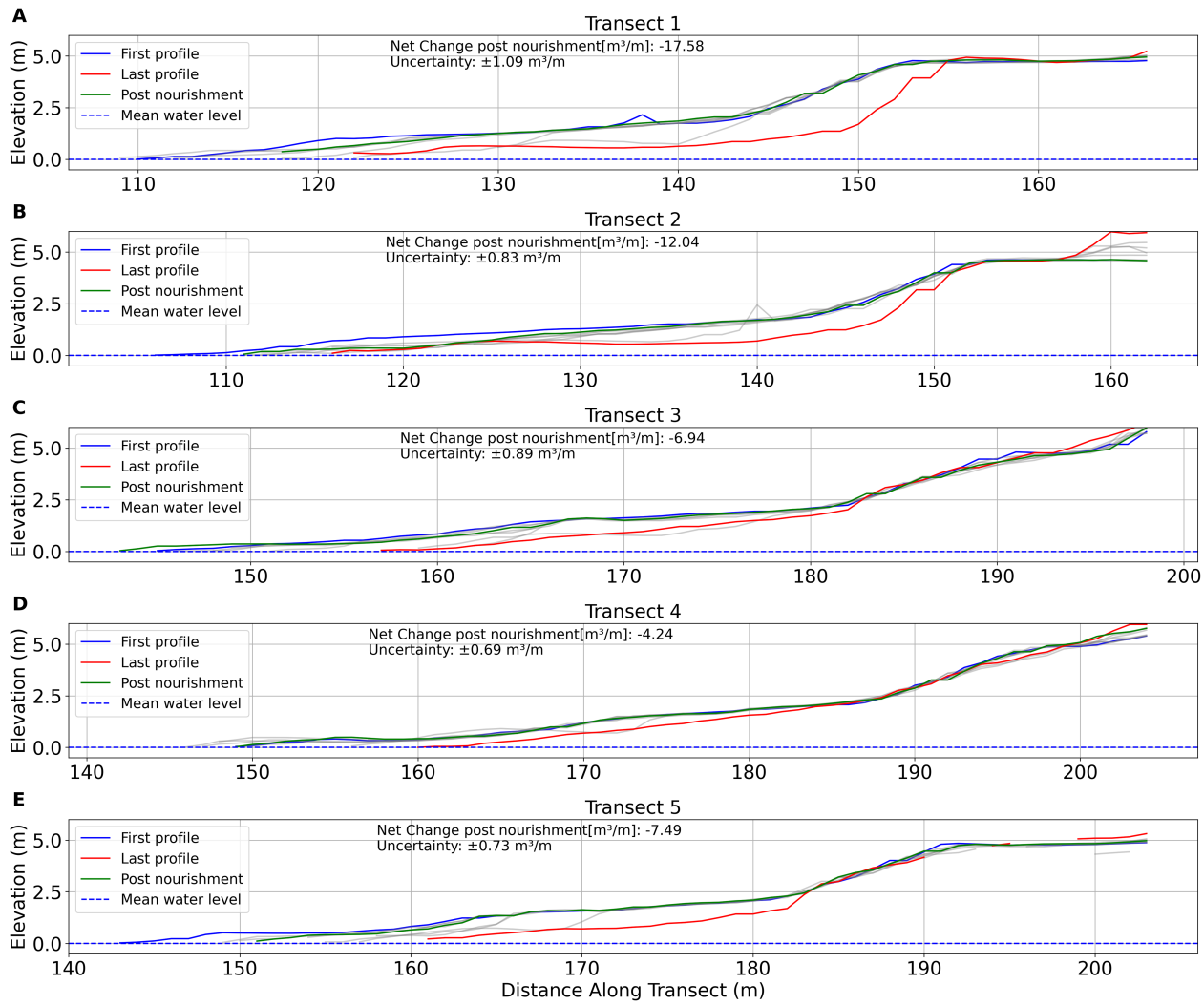

FIGURE 13
Medium-term monitoring of the aerial beach profile development in each transect from the UAV monitoring.

the shoreline in the southern part of the shoreline and found further offshore in the northern part, near the national park. This difference in coastal curvature and local metocean conditions likely influences the sandbar dynamics and their responses to nourishment.

In particular, the rapid development of sandbars in our study underscores the need for ongoing research into the effects of various nourishment strategies on coastal morphodynamics. While our findings demonstrate quicker sandbar development, further investigation is required to understand the protective role and long-term stability of these sandbars. This understanding is crucial for optimizing coastal protection strategies. Our study provides valuable insights into the diverse responses of sandbars to nourishment projects, emphasizing the importance of context-specific approaches in coastal engineering.

Due to the limited frequency of surveys, particularly the UAV surveys, establishing a direct relationship between beach changes and metocean forcing remains challenging. Additionally, the variability in survey timing, especially in relation to storm events, complicates assessments of storm impact on the beach, as surveys were not consistently conducted immediately before and after storm occurrences. Nevertheless, our surveys, which cover approx. two years, provide valuable insights into the seasonal and long-term development of the nourishment. To capture beach changes in response to metocean forcing with high temporal resolution, continuous monitoring, such as a fixed laser station, would be necessary. However, such an approach would also restrict beach access and entail funding as well as regulatory approvals.

In summary, our observations at Ahrenshoop reveal a faster and closer formation of sandbars post-nourishment compared to both de Schipper et al. (2016) and Radermacher et al. (2018). The development of a non-barred profile at Ahrenshoop contrasts with the barred profile at the Sand Engine, highlighting how different coastal and nourishment conditions can influence sandbar dynamics. The findings suggest that while the general principles of sand nourishment's impact on sandbar formation hold true, the specifics can vary significantly based on local conditions and implementation methods.

Accuracy

In recent years, UAV photogrammetry has emerged as a powerful tool for acquiring high-resolution geospatial data, offering unprecedented accuracy in mapping and 3D modeling. However, achieving consistently high precision in UAV photogrammetric applications requires careful consideration of various factors, including flight parameters, image acquisition techniques, and processing methodologies. However, it is important to note that the inclusion of oblique imagery did not uniformly enhance accuracy across all instances. For one measurement station, the deviation increased slightly by 0.01 m, indicating that while the general trend showed improved accuracy, there were isolated cases where oblique imagery introduced minor inconsistencies. This phenomenon suggests that while oblique imagery generally contributes positively to the accuracy, it may also introduce complexities that necessitate careful management to avoid introducing new errors.

Overall, these findings highlight the critical importance of advanced processing techniques in achieving high-precision geospatial data. The initial results from direct georeferencing underscore the need for enhanced processing methodologies to meet the stringent accuracy requirements of modern applications. The significant improvements brought by co-alignment and further augmented by oblique imagery integration demonstrate a robust approach for achieving precise vertical accuracy. Future applications and methodologies should continue to explore the optimization of these processes, particularly focusing on mitigating the minor inconsistencies observed when incorporating oblique imagery, to ensure consistently high-quality geospatial data.

It must be noted that in comparison to other studies, the study area is not shaped like a square but instead has a challenging elongated geometry. Also, the number of tie points in the area is much lower than found in other studies due to the high variability on the sandy beach, which occupies a major part of all the images. The difficulties in reproducing the height accurately can be referred to a miscalculation of the focal length of the camera as was also found in other studies (Benassi et al., 2017; Forlani et al., 2018).

Figuress 12A–C highlights key insights into the uncertainty of the measurements, particularly towards the end of the survey period. In both Figures 12A, B, the error bars representing uncertainty in volume change above and below MSL become notably larger as the survey progresses. This increase in uncertainty, especially towards the later stages, indicates a diminishing accuracy in the measurements.

Figure 12C, which shows the cumulative uncertainty for each transect, further emphasizes this issue. As uncertainties from each time step accumulate, the total uncertainty steadily increases. While the cumulative uncertainty remains manageable in the early stages, it becomes more significant by the end of the survey period. This compounding of errors highlights the growing challenge in accurately interpreting the results, as the cumulative uncertainty near the end makes the data less reliable.

In conclusion, while the early stages of the survey (as shown in Figures 12A, B) maintain reasonable accuracy, the steadily increasing cumulative uncertainty in Figure 12C, suggest that the results in the latter part of the survey should be interpreted with caution. The diminishing accuracy leaves the final measurements more uncertain, limiting the robustness of conclusions drawn from this period.

Conclusion

In conclusion, this study has provided a most valuable dataset of the evolution of nourishment over longer time spans. Key insights are provided by means of observation and evaluation of the morphological changes following beach nourishment. The seaward movement of the breaking point and sandbar, and the transformation of non-barred profiles into barred ones, highlight the dynamic response of the beach to sediment addition.

Connecting short-term terrestrial monitoring with medium-term UAV monitoring reveals the extended effects of sandbars on coastal dynamics. The data underscores that sandbars play a significant role in volumetric changes and overall beach dynamics. It is essential to closely monitor and understand sandbar dynamics when planning and implementing beach nourishment projects. Assessing whether nourishment interventions can positively influence sandbar development should be a standard consideration.

Methodologically, we demonstrated that co-alignment in photogrammetric processing is highly effective, enabling us to generate high-quality survey data even in a dynamic coastal environment, where deploying GCPs is impractical. By applying this approach, UAV surveys can efficiently cover extensive areas, which is particularly advantageous in such variable coastal settings. While other studies have successfully utilized co-alignment for river systems (de Haas et al., 2021) or for wetland areas (López and Cellone, 2022), our research demonstrates its applicability in coastal environments prone to constant morphological change. However, careful consideration of regulatory approvals is essential, particularly when conducting surveys over inhabited regions or protected natural areas.

Combining short-term monitoring of detailed changes in the subaqueous and subaerial segments of the beach profile with medium-term monitoring of the overall beach and dune system has proven essential for understanding the enduring impacts of nourishment activities. These insights are crucial for guiding future beach nourishment projects, demonstrating the value of integrating both high-resolution short-term observations and sustained monitoring. The strategic focus must be on optimizing the use of sand resources to ensure the best return on investment, thereby supporting sustainable coastal development and resilience. Such an approach supports sustainable coastal development while bolstering the adaptive capacity of these environments against future climate change.

Data availability statement

The data from the UAV surveys presented in the study are publicly available here: https://zenodo.org/records/14247159. The terrestrial data was obtained from the State Agency of Agriculture and Environment (StALU) in Germany. All requests and inquiries should be directed towards the StALU (https://www.stalu-mv.de/mm/).

Author contributions

JT: Writing – review & editing, Writing – original draft. CJ: Writing – review & editing. MS: Writing – review & editing. KS: Writing – review & editing. TS: Writing – review & editing.

Funding

The author(s) declare financial support was received for the research, authorship, and/or publication of this article. This research was conducted as part of the joint research project ECAS-Baltic which was funded by the German Federal Ministry of Education and Research under the funding code 03F0860E.

Acknowledgments

We thank the StALU for answering detailed questions about the coastal protection strategy of MWP and supplying the terrestrial dataset. The publication of this article was funded by the Open Access Fund of Leibniz Universität Hanover.

Conflict of interest

The authors declare that the research was conducted in the absence of any commercial or financial relationships that could be construed as a potential conflict of interest.

The author(s) declared that they were an editorial board member of Frontiers, at the time of submission. This had no impact on the peer review process and the final decision.

Publisher's note

Supplementary material

The Supplementary Material for this article can be found online at: https://www.frontiersin.org/articles/10.3389/fmars.2024.1473237/full#supplementary-material

References

Aagaard, T., Hughes, M., Møller-Sørensen, R., and Andersen, S. (2006). Hydrodynamics and sediment fluxes across an onshore migrating intertidal bar. *J. Coast. Res.* 22, 247–259. doi: 10.2112/04-0214.1

Aguilera-Vidal, M., Muñoz-Perez, J. J., Contreras, A., Contreras, F., Lopez-Garcia, P., and Jigena, B. (2022). Increase in the erosion rate due to the impact of climate change on sea level rise: victoria beach, a case study. *J. Mar. Sci. Eng.* 10, 1912. doi: 10.3390/jmse10121912

Barbier, E. B., Hacker, S. D., Kennedy, C., Koch, E. W., Stier, A. C., and Silliman, B. R. (2011). The value of estuarine and coastal ecosystem services. *Ecol. Monogr.* 81, 169–193. doi: 10.1890/10-1510.1

Battjes, J. A. (1974). "Surf Similarity," in *Coastal Engineering 1974* (American Society of Civil Engineers, Copenhagen, Denmark), 466–480. doi: 10.1061/9780872621138.029

Benassi, F., Dall'Asta, E., Diotri, F., Forlani, G., Morra di Cella, U., Roncella, R., et al. (2017). Testing accuracy and repeatability of UAV blocks oriented with GNSS-supported aerial triangulation. *Remote Sens.* 9, 172. doi: 10.3390/rs9020172

Björkqvist, J.-V., Lukas, I., Alari, V., van Vledder, G., Hulst, S., Pettersson, H., et al. (2018). Comparing a 41-year model hindcast with decades of wave measurements from the Baltic Sea. *Ocean Eng.* 152, 57–71. doi: 10.1016/j.oceaneng.2018.01.048

Browder, A. E., and Dean, R. G. (2000). Monitoring and comparison to predictive models of the Perdido Key beach nourishment project, Florida, USA. *Coast. Eng.* 39, 173–191. doi: 10.1016/S0378-3839(99)00057-5

Bruun, P. (1954). *Coast Erosion and the Development of Beach Profiles* (United States: Beach Erosion Board). Available online at: https://erdc-library.erdc.dren.mil/jspui/handle/11681/3426 (Accessed August 21, 2023).

BSH - Seegang (2024). Available online at: https://www.bsh.de/DE/DATEN/Klima-und-Meer/Seegang/seegang_node.html (Accessed August 31, 2024).

Cai, F., Dean, R., and Liu, J. (2011). "Beach nourishment in China: Status and prospects," in *Proceedings of the International Conference on Coastal Engineering: No 32 (2010): Proceedings of 32nd Conference on Coastal Engineering, Shanghai, China, 2010.; management.31 1*. doi: 10.9753/icce.v32.management.31

Cheney, E. W., and Kincaid, D. (1998). *Numerical Mathematics and Computing. 4th ed.* (Pacific Grove, CA: Brooks/Cole Pub. Co.).

Cohn, N., Anderson, D., and Ruggiero, P. (2015). "Observations of intertidal bar welding along a high energy, dissipative coastline," in *The proceedings of the coastal sediments 2015* (San Diego, USA: WORLD SCIENTIFIC). doi: 10.1142/9789814689977_0021

Contreras-de-Villar, F., García, F. J., Muñoz-Perez, J. J., Contreras-de-Villar, A., Ruiz-Ortiz, V., Lopez, P., et al. (2021). Beach leveling using a remotely piloted aircraft system (RPAS): problems and solutions. *J. Mar. Sci. Eng.* 9, 19. doi: 10.3390/jmse9010019

Cook, K. L., and Dietze, M. (2019). Short Communication: A simple workflow for robust low-cost UAV-derived change detection without ground control points. *Earth Surface Dynamics* 7, 1009–1017. doi: 10.5194/esurf-7-1009-2019

David, C. G., Kohl, N., Casella, E., Rovere, A., Ballesteros, P., and Schlurmann, T. (2021). Structure-from-Motion on shallow reefs and beaches: potential and limitations of consumer-grade drones to reconstruct topography and bathymetry. *Coral Reefs* 40, 835–851. doi: 10.1007/s00338-021-02088-9

Dean, R. G. (1977). Equilibrium beach profiles: US Atlantic and Gulf coasts. *Ocean Engineering Report 12.*

Dean, R. (1987).Coastal sediment processes: Toward coastal engineering solutions. In: *Spec. Conf. Understanding Coastal Sediment Processes* (New York: ASCE). Available online at: https://www.google.com/search?q=Dean%2C+R.+1987.+Coastal+sediment+processes%3A+Toward+coastal+engineering+solutions.+Spec.+Conf.+Understanding+Coastal+Sediment+Processes.+N.C.+Kraus%2C+ed.+ASCE%2C+New+York%2C+pp.+1-24&rlz=1C1ONGR_deDE1061DE1061&sourceid=chrome&ie=UTF-8 (Accessed August 21, 2023).

Dean, R. G. (2002). *Beach nourishment: theory and practice* (River Edge, NJ: World Scientific).

de Haas, T., Nijland, W., McArdell, B. W., and Kalthof, M. W. M. L. (2021). Case report: optimization of topographic change detection with UAV structure-from-

motion photogrammetry through survey co-alignment. *Front. Remote Sens.* 2. Available at: https://www.frontiersin.org/articles/10.3389/frsen.2021.626810.

de Schipper, M. A., de Vries, S., Ruessink, G., de Zeeuw, R. C., Rutten, J., van Gelder-Maas, C., et al. (2016). Initial spreading of a mega feeder nourishment: Observations of the Sand Engine pilot project. *Coast. Eng.* 111, 23–38. doi: 10.1016/j.coastaleng.2015.10.011

Elko, N. A., and Wang, P. (2007). Immediate profile and planform evolution of a beach nourishment project with hurricane influences. *Coast. Eng.* 54, 49–66. doi: 10.1016/j.coastaleng.2006.08.001

European Commission (2022). *The EU blue economy report 2022* (Publications Office). Available online at: https://data.europa.eu/doi/10.2771/793264 (Accessed February 8, 2024).

Everard, M., Jones, L., and Watts, B. (2010). Have we neglected the societal importance of sand dunes? An ecosystem services perspective. *Aquat. Conservation: Mar. Freshw. Ecosyst.* 20, 476–487. doi: 10.1002/aqc.1114

Feistel, R., Weinreben, S., Wolf, H., Seitz, S., Spitzer, P., Adel, B., et al. (2010). Density and absolute salinity of the baltic sea 2006–2009. *Ocean Sci.* 6, 3–24. doi: 10.5194/os-6-3-2010

Fisher, P. F., and Tate, N. J. (2006). Causes and consequences of error in digital elevation models. *Prog. Phys. Geography: Earth Environ.* 30, 467–489. doi: 10.1191/0309133306pp492ra

Fontán-Bouzas, Á., Andriolo, U., Silva, P. A., and Baptista, P. (2022). Wave impact analysis on a beach-dune system to support coastal management and nourishment works: the showcase of mira, Portugal. *Front. Mar. Sci.* 9. Available at: https://www.frontiersin.org/articles/10.3389/fmars.2022.861569.

Forlani, G., Dall'Asta, E., Diotri, F., Cella, U. M. D., Roncella, R., and Santise, M. (2018). Quality assessment of DSMs produced from UAV flights georeferenced with on-board RTK positioning. *Remote Sens.* 10, 311. doi: 10.3390/rs10020311

Fröhle, P., and Dimke, S. (2008). "Analysis of potential long shore sediment transport at the coast of Mecklenburg-Vorpommern," in *Proc. Chinese-German Joint Symposium on Hydraulic and Ocean Engineering*, Darmstadt, Germany, August 24-30, 2008.

Gabara, G., and Sawicki, P. (2019). Multi-variant accuracy evaluation of UAV imaging surveys: A case study on investment area. *Sensors* 19, 5229. doi: 10.3390/s19235229

Gares, P. A., Wang, Y., and White, S. A. (2006). Using LIDAR to monitor a beach nourishment project at wrightsville beach, North Carolina, USA. *coas* 2006, 1206–1219. doi: 10.2112/06A-0003.1

Gijsman, R., Ruessink, B., Visscher, J., and Schlurmann, T. (2021). Observations on decadal sandbar behaviour along a large-scale curved shoreline. *Earth Surface Processes Landforms* 46, 490–503. doi: 10.1002/esp.5041

Gindraux, S., Boesch, R., and Farinotti, D. (2017). Accuracy assessment of digital surface models from unmanned aerial vehicles' Imagery on glaciers. *Remote Sens.* 9, 186. doi: 10.3390/rs9020186

Ghanavati, M., Young, I., Kirezci, E., Ranasinghe, R., Duong, T. M., and Luijendijk, A. P. (2023). An assessment of whether long-term global changes in waves and storm surges have impacted global coastlines. *Sci. Rep.* 13, 11549. doi: 10.1038/s41598-023-38729-y

Glueck, D., and Schubert, H. (2024). "Suspended particle dynamics during sand nourishments and storm events: A comparative analysis," in *Sediment transport research - further recent advances*. Ed. A. J. Manning (IntechOpen), 1-20. doi: 10.5772/intechopen.1004905

Holthuijsen, L. H. (2007). *Waves in Oceanic and Coastal Waters* (Cambridge: Cambridge University Press). doi: 10.1017/CBO9780511618536

Hugenholtz, C. H., Whitehead, K., Brown, O. W., Barchyn, T. E., Moorman, B. J., LeClair, A., et al. (2013). Geomorphological mapping with a small unmanned aircraft system (sUAS): Feature detection and accuracy assessment of a photogrammetrically-derived digital terrain model. *Geomorphology* 194, 16–24. doi: 10.1016/j.geomorph.2013.03.023

Jackson, N. L., Nordstrom, K. F., Saini, S., and Smith, D. R. (2010). Effects of nourishment on the form and function of an estuarine beach. *Ecol. Eng.* 36, 1709–1718. doi: 10.1016/j.ecoleng.2010.07.016

James, M. R., and Robson, S. (2014). Mitigating systematic error in topographic models derived from UAV and ground-based image networks. *Earth Surface Processes Landforms* 39, 1413–1420. doi: 10.1002/esp.3609

Jeong, E., Park, J.-Y., and Hwang, C.-S. (2018). Assessment of UAV photogrammetric mapping accuracy in the beach environment. *J. Coast. Res.* 85, 176–180. doi: 10.2112/SI85-036.1

Kelln, J., Dangendorf, S., Gräwe, U., Steffen, H., and Jensen, J. (2022). Entwicklung des mittleren Meeresspiegels entlang der südwestlichen Ostseeküste. *Die Küste* 91, 181–220. doi: 10.18171/1.091107

Komar, P. D., and Inman, D. L. (1970). Longshore sand transport on beaches. *J. Geophysical Res. (1896-1977)* 75, 5914–5927. doi: 10.1029/JC075i030p05914

Kortekaas, S., Bagdanaviciute, I., Gyssels, P., Huerta, J. M. A., and Héquette, A. (2010). Assessment of the effects of marine aggregate extraction on the coastline: an example from the german baltic sea coast. *J. Coast. Res.* 51, 205–214. doi: 10.2307/40928832

Lane, S. N., Westaway, R. M., and Murray Hicks, D. (2003). Estimation of erosion and deposition volumes in a large, gravel-bed, braided river using synoptic remote sensing. *Earth Surface Processes Landforms* 28, 249–271. doi: 10.1002/esp.483

Larson, M., Hanson, H., Kraus, N. C., and Newe, J. (1999). Short- and long-term responses of beach fills determined by eof analysis. *J. Waterw. Port Coast. Ocean Eng.*125, 285–293. doi: 10.1061/(ASCE)0733-950X(1999)125:6(285)

Leach, C., Kennedy, D. M., Pucino, N., Doumtsis, S., Sorrell, K., Allan, B., et al. (2023). Measuring drivers of shoreline and subaerial beach change using limited datasets in a temperate, wave-dominated sandy system: Inverloch, Australia. *Ocean Coast. Manage.* 240, 106641. doi: 10.1016/j.ocecoaman.2023.106641

Leatherman, S. P., Zhang, K., and Douglas, B. C. (2000). Sea level rise shown to drive coastal erosion. *Eos Trans. Am. Geophysical Union* 81, 55–57. doi: 10.1029/00EO00034

Leont'ev, I. O. (2011). Submarine bars on sandy coasts. *Oceanology* 51, 141–147. doi: 10.1134/S0001437011010115

López, L., and Cellone, F. (2022). SfM-MVS and GIS analysis of shoreline changes in a coastal wetland, Parque Costero del Sur biosphere reserve, Argentina. *Geocarto Int.* 37, 11134–11150. doi: 10.1080/10106049.2022.2046870

Ludka, B. C., Young, A. P., Guza, R. T., O'Reilly, W. C., and Merrifield, M. A. (2023). Alongshore variability of a southern California beach, before and after nourishment. *Coast. Eng.* 179, 104223. doi: 10.1016/j.coastaleng.2022.104223

Luijendijk, A. P., Ranasinghe, R., De Schipper, M. A., Huisman, B. A., Swinkels, C. M., Walstra, D. J. R., et al. (2017). The initial morphological response of the Sand Engine: A process-based modelling study. *Coast. Eng.* 119, 1–14. doi: 10.1016/j.coastaleng.2016.09.005

Madsen, K. S., Høyer, J. L., Fu, W., and Donlon, C. (2015). Blending of satellite and tide gauge sea level observations and its assimilation in a storm surge model of the North Sea and Baltic Sea. *J. Geophysical Res. (Oceans)* 120, 6405–6418. doi: 10.1002/2015JC011070

Madsen, K. S., Høyer, J. L., Suursaar, Ü., She, J., and Knudsen, P. (2019). Sea level trends and variability of the baltic sea from 2D statistical reconstruction and altimetry. *Front. Earth Sci.* 7. doi: 10.3389/feart.2019.00243

Manfreda, S., Dvorak, P., Mullerova, J., Herban, S., Vuono, P., Arranz Justel, J. J., et al. (2019). Assessing the accuracy of digital surface models derived from optical imagery acquired with unmanned aerial systems. *Drones* 3, 15. doi: 10.3390/drones3010015

McGill, S. P., Harris, B. D., McFall, B. C., Krafft, D. R., Bain, R. L., Olsen, N. R., et al. (2022). Morphological analysis of a nearshore nourishment along the atlantic coast of New Jersey, USA. *J. Mar. Sci. Eng.* 10, 1622. doi: 10.3390/jmse10111622

Melito, L., Parlagreco, L., Perugini, E., Postacchini, M., Zitti, G., Brocchini, M., et al. (2018). "Monitoring for coastal resilience: A project for five Italian beaches," in *2018 IEEE International Workshop on Metrology for the Sea; Learning to Measure Sea Health Parameters (MetroSea)*. (Bari, Italy: IEEE), 76-81. doi: 10.1109/MetroSea.2018.8657838

Mentaschi, L., Vousdoukas, M. I., Pekel, J.-F., Voukouvalas, E., and Feyen, L. (2018). Global long-term observations of coastal erosion and accretion. *Sci. Rep.* 8, 12876. doi: 10.1038/s41598-018-30904-w

Monioudi, I. N., Velegrakis, A. F., Chatzipavlis, A. E., Rigos, A., Karambas, T., Vousdoukas, M. I., et al. (2017). Assessment of island beach erosion due to sea level rise: the case of the Aegean archipelago (Eastern Mediterranean). *Natural Hazards Earth System Sci.* 17, 449–466. doi: 10.5194/nhess-17-449-2017

Muñoz-Pérez, J., Medina, R., and Tejedor, B. (2001). Evolution of longshore beach contour lines determined by EOF method. *Scientia Marina* 65, 393–402. doi: 10.3989/scimar.2001.65n4393

Muñoz-Pérez, J., Payo, A., Roman-Sierra, J., Navarro-Pons, M., and Moreno, L. (2012). Optimization of beach profile spacing: An applicable tool for coastal monitoring. *Scientia Marina* 76, 791–798. doi: 10.3989/scimar.03417.15A

Neugirg, F. (2016). Using terrestrial LiDAR data to analyse morphodynamics on steep unvegetated slopes driven by different geomorphic processes. *Catena: an Interdiscip. J. Soil science hydrology geomorphology focusing geoecology Landscape Evol.* 142, 269–280. doi: 10.1016/j.catena.2016.03.021

Nota, E. W., Nijland, W., and de Haas, T. (2022). Improving UAV-SfM time-series accuracy by co-alignment and contributions of ground control or RTK positioning. *Int. J. Appl. Earth Observation Geoinformation* 109, 102772. doi: 10.1016/j.jag.2022.102772

Ojeda, E., and Guillén, J. (2006). Monitoring beach nourishment based on detailed observations with video measurements. *J. Coast. Res.*, 100–106. Available online at: https://www.jstor.org/stable/25737388.

Oppenheimer, M., Glavovic, B. C., Hinkel, J., van de Wal, R., Magnan, A. K., Abd-Elgawad, A., et al. (2019). *Sea Level Rise and Implications for Low-Lying Islands, Coasts and Communities* (Cambridge, UK and New York, US: IPCC). Available at: https://www.cambridge.org/core/product/identifier/9781009157964/type/book.

Peterson, C. H., and Bishop, M. J. (2005). Assessing the environmental impacts of beach nourishment. *BioScience* 55, 887–896. doi: 10.1641/0006-3568(2005)055[0887:ATEIOB]2.0.CO;2

Quartel, S., Kroon, A., and Ruessink, B. G. (2008). Seasonal accretion and erosion patterns of a microtidal sandy beach. *Mar. Geology* 250, 19–33. doi: 10.1016/j.margeo.2007.11.003

Radermacher, M., de Schipper, M. A., Price, T. D., Huisman, B. J. A., Aarninkhof, S. G. J., and Reniers, A. J. H. M. (2018). Behaviour of subtidal sandbars in response to nourishments. *Geomorphology* 313, 1–12. doi: 10.1016/j.geomorph.2018.04.005

Reckermann, M., Omstedt, A., Soomere, T., Aigars, J., Akhtar, N., Bełdowska, M., et al. (2022). Human impacts and their interactions in the Baltic Sea region. *Earth System Dynamics* 13, 1–80. doi: 10.5194/esd-13-1-2022

Saengsupavanich, C., Pranzini, E., Ariffin, E. H., and Yun, L. S. (2023). Jeopardizing the environment with beach nourishment. *Sci. Total Environ.* 868, 161485. doi: 10.1016/j.scitotenv.2023.161485

Sallenger, A. H. Jr (2000). Storm impact scale for barrier islands. *J. Coast. Res.* 16, 890–895. Available online at: https://www.jstor.org/stable/4300099.

Schoonees, T., Gijón Mancheño, A., Scheres, B., Bouma, T. J., Silva, R., Schlurmann, T., et al. (2019). Hard structures for coastal protection, towards greener designs. *Estuaries Coasts* 42, 1709–1729. doi: 10.1007/s12237-019-00551-z

Shand, R. D. (2003). Relationships between episodes of bar switching, cross-shore bar migration and outer bar degeneration at Wanganui, New Zealand. *J. Coast. Res.* 19, 157–170. Available online at: https://www.jstor.org/stable/4299154.

StALU (2021). Regelwerk Küstenschutz Mecklenburg-Vorpommern. Available online at: https://www.stalu-mv.de/mm/Themen/K%C3%BCstenschutz/Regelwerk-K%C3%BCstenschutz-Mecklenburg%E2%80%93Vorpommern/ (Accessed September 7, 2024).

Staudt, F., Gijsman, R., Ganal, C., Mielck, F., Wolbring, J., Hass, H. C., et al. (2021). The sustainability of beach nourishments: a review of nourishment and environmental monitoring practice. *J. Coast. Conserv.* 25, 34. doi: 10.1007/s11852-021-00801-y

Stockdon, H. F., Holman, R. A., Howd, P. A., and Sallenger, A. H. (2006). Empirical parameterization of setup, swash, and runup. *Coast. Eng.* 53, 573–588. doi: 10.1016/j.coastaleng.2005.12.005

Štroner, M., Urban, R., Reindl, T., Seidl, J., and Brouček, J. (2020). Evaluation of the georeferencing accuracy of a photogrammetric model using a quadrocopter with onboard GNSS RTK. *Sensors* 20, 2318. doi: 10.3390/s20082318

Štroner, M., Urban, R., Seidl, J., Reindl, T., and Brouček, J. (2021). Photogrammetry using UAV-mounted GNSS RTK: georeferencing strategies without GCPs. *Remote Sens.* 13, 1336. doi: 10.3390/rs13071336

Suursaar, Ü., Kullas, T., Otsmann, M., Saaremäe, I., Kuik, J., and Merilain, M. (2006). Cyclone Gudrun in January 2005 and modelling its hydrodynamic consequences in the Estonian coastal waters. *Boreal Environ. Res.* 11, 143. Available at: http://www.borenv.net/BER/archive/pdfs/ber11/ber11-143.pdf.

Vos, K., Splinter, K. D., Harley, M. D., Simmons, J. A., and Turner, I. L. (2019). CoastSat: A Google Earth Engine-enabled Python toolkit to extract shorelines from publicly available satellite imagery. *Environ. Model. Software* 122, 104528. doi: 10.1016/j.envsoft.2019.104528

Weisse, R., Dailidienė, I., Hünicke, B., Kahma, K., Madsen, K., Omstedt, A., et al. (2021). Sea level dynamics and coastal erosion in the Baltic Sea region. *Earth System Dynamics* 12, 871–898. doi: 10.5194/esd-12-871-2021

Wheaton, J. M., Brasington, J., Darby, S. E., and Sear, D. A. (2010). Accounting for uncertainty in DEMs from repeat topographic surveys: improved sediment budgets. *Earth Surface Processes Landforms* 35, 136–156. doi: 10.1002/esp.1886

Wijnberg, K. M., and Terwindt, J. H. J. (1995). Extracting decadal morphological behaviour from high-resolution, long-term bathymetric surveys along the Holland coast using eigenfunction analysis. *Mar. Geology* 126, 301–330. doi: 10.1016/0025-3227(95)00084-C

Wolski, T., Wiśniewski, B., Giza, A., Kowalewska-Kalkowska, H., Boman, H., Grabbi-Kaiv, S., et al. (2014). Extreme sea levels at selected stations on the Baltic Sea coast*. *Oceanologia* 56, 259–290. doi: 10.5697/oc.56-2.259

Wright, L. D., and Short, A. D. (1984). Morphodynamic variability of surf zones and beaches: A synthesis. *Mar. Geology* 56, 93–118. doi: 10.1016/0025-3227(84)90008-2

Yuhi, M., and Umeda, S. (2018). Characteristics of systematic migrations of multiple sandbars and related cross-shore sediment transport at chirihama and adjacent coasts, Japan. *coas* 85, 231–235. doi: 10.2112/SI85-047.1